


RESEARCH ARTICLE

Leaf nitrogen from the perspective of optimal plant function

Ning Dong^{1,2}  | Iain Colin Prentice^{1,2,3}  | Ian J. Wright^{2,4}  | Han Wang³  |
Owen K. Atkin⁵  | Keith J. Bloomfield¹ | Tomas F. Domingues⁶  | Sean M. Gleason⁷  |
Vincent Maire⁸  | Yusuke Onoda⁹  | Hendrik Poorter^{2,10}  | Nicholas G. Smith¹¹ 

¹Department of Life Sciences, Georgina Mace Centre for the Living Planet, Imperial College London, Ascot, UK; ²Department of Biological Sciences, Macquarie University, Sydney, New South Wales, Australia; ³Ministry of Education Key Laboratory for Earth System Modelling, Department of Earth System Science, Tsinghua University, Beijing, China; ⁴Hawkesbury Institute for the Environment, Western Sydney University, Penrith, New South Wales, Australia; ⁵Australian Research Council Centre of Excellence in Plant Energy Biology, Research School of Biology, The Australian National University, Canberra, Australian Capital Territory, Australia; ⁶FFCLRP, Department of Biology, University of São Paulo, Ribeirão Preto, Brazil; ⁷Water Management and Systems Research Unit, USDA-ARS, Fort Collins, Colorado, USA; ⁸Département des sciences de l'environnement, Université du Québec à Trois-Rivières, Trois-Rivières, Québec, Canada; ⁹Graduate School of Agriculture, Kyoto University, Kyoto, Japan; ¹⁰Plant Sciences (IBG-2), Forschungszentrum Jülich GmbH, Jülich, Germany and ¹¹Department of Biological Sciences, Texas Tech University, Lubbock, Texas, USA

Correspondence

Ning Dong

Email: n.dong@imperial.ac.uk

Funding information

Australian Research Council, Grant/Award Number: DP170103410; H2020 European Research Council, Grant/Award Number: 787203 REALM; Schmidt Family Foundation; LEMONTREE

Handling Editor: Imma Oliveras Menor

Abstract

1. Leaf dry mass per unit area (LMA), carboxylation capacity (V_{cmax}) and leaf nitrogen per unit area (N_{area}) and mass (N_{mass}) are key traits for plant functional ecology and ecosystem modelling. There is however no consensus about how these traits are regulated, or how they should be modelled. Here we confirm that observed leaf nitrogen across species and sites can be estimated well from observed LMA and V_{cmax} at 25°C ($V_{\text{cmax}25}$). We then test the hypothesis that global variations of both quantities depend on climate variables in specific ways that are predicted by leaf-level optimality theory, thus allowing both N_{area} to be predicted as functions of the growth environment.
2. A new global compilation of field measurements was used to quantify the empirical relationships of leaf N to $V_{\text{cmax}25}$ and LMA. Relationships of observed $V_{\text{cmax}25}$ and LMA to climate variables were estimated, and compared to independent theoretical predictions of these relationships. Soil effects were assessed by analysing biases in the theoretical predictions.
3. LMA was the most important predictor of N_{area} (increasing) and N_{mass} (decreasing). About 60% of global variation across species and sites in observed N_{area} , and 31% in N_{mass} , could be explained by observed LMA and $V_{\text{cmax}25}$. These traits, in turn, were quantitatively related to climate variables, with significant partial relationships similar or indistinguishable from those predicted by optimality theory. Predicted trait values explained 21% of global variation in observed site-mean $V_{\text{cmax}25}$, 43% in LMA and 31% in N_{area} . Predicted $V_{\text{cmax}25}$ was biased low on clay-rich soils but predicted LMA was biased high, with compensating effects on N_{area} . N_{area} was overpredicted on organic soils.

This is an open access article under the terms of the [Creative Commons Attribution-NonCommercial-NoDerivs](https://creativecommons.org/licenses/by-nc-nd/4.0/) License, which permits use and distribution in any medium, provided the original work is properly cited, the use is non-commercial and no modifications or adaptations are made.

© 2022 The Authors. *Journal of Ecology* published by John Wiley & Sons Ltd on behalf of British Ecological Society.

4. *Synthesis*. Global patterns of variation in observed site-mean N_{area} can be explained by climate-induced variations in optimal $V_{\text{cmax}25}$ and LMA. Leaf nitrogen should accordingly be modelled as a consequence (not a cause) of $V_{\text{cmax}25}$ and LMA, both being optimized to the environment. Nitrogen limitation of plant growth would then be modelled principally via whole-plant carbon allocation, rather than via leaf-level traits. Further research is required to better understand and model the terrestrial nitrogen and carbon cycles and their coupling.

KEYWORDS

coordination hypothesis, ecosystem model, leaf mass per area, leaf nitrogen, least-cost hypothesis, nitrogen cycle, photosynthetic capacity

1 | INTRODUCTION

An influential review (Field & Mooney, 1986) helped to establish the relationship between leaf nitrogen (N) and photosynthesis as a cornerstone of modern ecophysiological theory. Drawing on previous empirical studies and reviews, Field and Mooney (1986) considered the implications of observed correlations between the light-saturated photosynthetic rate (as a measure of photosynthetic capacity) and leaf N content, expressed on either an area or a mass basis. Numerous studies have confirmed the positive correlation between photosynthesis and leaf N at local, regional and global scales (see e.g. Evans, 1989; Niinemets, 1999; Wright et al., 2005). The correlation exists because photosynthetic processes depend on N-rich enzymes, and these—most importantly the primary carbon-fixing enzyme, ribulose-1,5-bisphosphate carboxylase/oxygenase (Rubisco)—comprise a substantial proportion of leaf N.

A heuristic stemming from work on herbaceous crops (Evans, 1983; Evans & Seemann, 1989) is that photosynthetic proteins together account for 50%–60% of leaf N, of which Rubisco alone accounts for 25–30%. In non-crop and woody species, however, Rubisco often contributes a smaller percentage of total leaf N than in crops. A recent estimated of N partitioning in a 'typical' C_3 leaf put the Rubisco contribution at 20%, and total photosynthetic N (in light-absorbing pigments, electron-transport proteins and enzymes of the Calvin cycle including Rubisco) at 54% of leaf N (Evans & Clarke, 2018). Onoda et al. (2017) indicated that Rubisco contributed on average <15% of leaf N across 70 woody evergreen species. They estimated mean N in cell walls as 15% of leaf N in woody evergreens (as large a contribution as Rubisco), and 11% across all species. They also found that the proportion of leaf N allocated to cell walls increases with leaf dry mass per unit area (LMA), pointing to the importance of structural as well as metabolic components of leaf N.

The representation of N cycling, with implications for primary production and its response to rising atmospheric CO_2 and regional N deposition, has become a priority in the development of dynamic global vegetation models (DGVMs)—including both 'offline' and coupled DGVMs (Meyerholt et al., 2020; Zaehle & Dalmonech, 2011). However, current DGVMs show large differences in their modelled

responses of primary production to carbon dioxide (CO_2) and N enhancement, reflecting a fundamental lack of agreement on the processes involved (Davies-Barnard et al., 2020). Key areas that are not well understood include the controls of gains and losses of reactive nitrogen at the ecosystem level, and the relative importance of nitrogen supply (from the soil, and/or N-fixing symbionts) and demand (by plants) in determining leaf N. Many coupled carbon–nitrogen (C–N) models can reproduce the CO_2 -induced enhancement of tree growth in Free Air Carbon Enrichment (FACE) experiments but have been shown to do so via the wrong mechanism, that is, they rely on shifts in leaf-level stoichiometry to reduce N demand (Finzi et al., 2007; Medlyn et al., 2015; Zaehle et al., 2014) rather than increasing N uptake, which is the principal mechanism at the Duke Forest and Oak Ridge FACE sites (Medlyn et al., 2015; Norby et al., 2010; Zaehle et al., 2014). Dong, Wright, et al. (2022) quantified leaf-level N declines in response to CO_2 enrichment; however, increased NPP nonetheless creates increased N demand at the whole-plant level. Many C–N models rely on the hypothesis that photosynthetic capacity is determined by leaf N (Walker et al., 2014; Zaehle & Dalmonech, 2011), which, in turn, is determined by soil N availability (Luo et al., 2004). The causality of these relationships is open to question, however. They have not been extensively tested.

A perspective on plant functional traits based on eco-evolutionary optimality theory (Franklin et al., 2020; Harrison et al., 2021) suggests an alternative approach to the interpretation and modelling of leaf N, which we explore in this paper. We start from the observation that leaf N per unit leaf area (N_{area}) is related to the amount of leaf tissue (indexed by LMA) and its metabolic activity (indexed by carboxylation capacity at 25°C, known as $V_{\text{cmax}25}$). Then, we test the hypothesis that both LMA and $V_{\text{cmax}25}$ adjust to the growth environment through some combination of phenotypic acclimation, genetic adaptation and environmental selection (Dong et al., 2020; Kikuzawa et al., 2013; Smith et al., 2019; Wang et al., 2017), approaching predictable community-mean values. V_{cmax} is predicted here by combining the coordination hypothesis (Chen et al., 1993; Dong et al., 2017; Peng et al., 2021; Smith et al., 2019; Togashi et al., 2018)—that V_{cmax} at growth temperatures acclimates so that photosynthesis

is (on average) neither limited by light nor by Rubisco activity—with the least-cost hypothesis—that stomatal behaviour minimizes the combined costs of maintaining both V_{cmax} and the water-transport pathway required to meet transpirational demand. Both costs can be expressed as functions of χ , the ratio of leaf internal to ambient CO_2 , allowing the optimal χ to be predicted from environmental variables (Prentice et al., 2014). The value of χ , in turn, determines how large V_{cmax} must be, to satisfy the coordination hypothesis (Wang et al., 2017). LMA is predicted here via a model based on Kikuzawa's (1991) hypothesis that leaf life span maximizes lifetime-average net carbon gain after deduction of amortized construction costs, Wang et al. (2021) extended this hypothesis to a prediction of how the leaf economics spectrum (the relationship between LMA and leaf life span), and the expected distribution of LMA values, shift as a function of the growth environment.

Dong et al. (2017) showed that more than half of the variance in N_{area} across multiple plant types and environments in Australia could be accounted for by a linear combination of measured LMA and optimal $V_{\text{cmax}25}$ values as predicted via the coordination hypothesis. A similar approach has been used to predict observed trends in N_{area} , based on field measurements of both quantities, along regional transects in the Andes (South America) and Gongga (western China) mountains, respectively (Peng et al., 2020; Xu et al., 2021). Here we present an analysis of a large, newly compiled global leaf N dataset, with associated gas-exchange measurements for all species. Our analysis proceeded in steps as follows. First, we analysed how leaf N depends statistically on measured LMA and $V_{\text{cmax}25}$, thereby testing and quantifying Dong et al.'s (2017) hypothesis—that N_{area} can be well approximated as the sum of components proportional to $V_{\text{cmax}25}$ and LMA, respectively—at a global scale. Second, we analysed how variations in site-mean $V_{\text{cmax}25}$ and LMA depend statistically on climate, and compared these empirical dependencies with those independently predicted by leaf-level optimality theory. Combining these first two steps, we then tested the extent to which variations in site-mean N_{area} could be predicted from climate via independently predicted site-mean values of $V_{\text{cmax}25}$ and LMA. Noting the evidence for effects of soil fertility factors on optimal leaf traits (Paillasa et al., 2020), we also analysed the extent to which deviations from climate-based predictions for $V_{\text{cmax}25}$, LMA and N_{area} were linked to soil clay content, pH and C:N ratio as an inverse proxy for N availability.

Our analysis focuses principally on N_{area} because of its relationship to photosynthetic light absorption. However, we carried out additional statistical analyses of leaf N per unit mass (N_{mass}), which relates to tissue stoichiometry and (unlike N_{area}) is measured independently of LMA. Osnas et al. (2013) provided a theoretical analysis of the relative merits of area- and mass-based expressions of leaf nutrients and photosynthetic traits. They indicated that area-based expressions were generally more appropriate, but also that leaf N includes both an area-proportional and a mass-proportional component, consistent with our approach.

2 | MATERIALS AND METHODS

2.1 | Trait data

A global dataset of observed V_{cmax} ($\mu\text{mol m}^{-2} \text{s}^{-1}$), N_{area} (g m^{-2}), N_{mass} (g g^{-1}) and LMA (g m^{-2}) values in field-grown mature C_3 plants—excluding crops (which, we surmised, might show different trait–trait and trait–environment relationships due to high levels of N fertilization) and C_4 and CAM plants—was assembled by merging the independent sets of measurements in several previous data compilations by the authors with additional data from literature. For details of source datasets, see Table S1. Figure S1 shows the distribution of samples in geographical and climatic space. In total, the measurements cover 3091 species at 300 sites. The data analysed for each site are mean trait values for all sampled individuals of each species. We also analysed site-mean trait values, as simple averages of species-mean values over all species present. Information on plant growth form, N-fixation status, phenological type (deciduous/evergreen) and photosynthetic pathway was obtained from source studies or the TRY database (Kattge et al., 2020). The term 'woody' here refers to tree, shrub, liana and hemiepiphyte growth forms.

Standard practice as described in the published sampling protocols has been to sample fully mature, outer-canopy leaves exposed to direct sunlight. However, leaves sampled in the outer canopy of understory species may receive little sunlight (Keenan & Niinemets, 2016). This is potentially problematic for large-scale analyses because field data generally include species at all canopy levels, while the specific light climates of the sampled leaves are unknown. Following Dong et al. (2017), we circumvented this problem by basing our independent theoretical predictions on a measure of canopy-average light availability (I_L), which declined relative to top-of-canopy light availability (I_0) as vegetation cover increases.

In some source datasets (e.g. Bloomfield et al., 2019), measurements were made on plants during very hot or dry periods, including plants suffering severe water stress. We adopted a conservative approach to removing measurements taken under extreme conditions, filtering out gas-exchange measurements indicating leaf-internal CO_2 concentration $< 60 \mu\text{mol mol}^{-1}$ or stomatal conductance $< 10 \text{mmol m}^{-2} \text{s}^{-1}$, which suggest a breakdown of leaf function. We also removed records of $N_{\text{area}} < 0.01 \text{g m}^{-2}$, which we assumed to be in error.

V_{cmax} values were derived from individual field-measured CO_2 response ($A-c_i$) curves or, when these were lacking, estimated from field measurements of light-saturated photosynthetic rate (A_{sat} , $\mu\text{mol m}^{-2} \text{s}^{-1}$), day respiration (R_{day} , $\mu\text{mol m}^{-2} \text{s}^{-1}$), leaf-internal CO_2 partial pressure (c_i , Pa) and leaf temperature (T , K) by the one-point method (De Kauwe et al., 2016). The use of this method can sometimes lead to underestimation of V_{cmax} (Burnett et al., 2019). The reported errors however do not exceed about 20%, indicating that the method is useful for large-scale surveys. The one-point formula is:

$$V_{\text{cmax}} = (A_{\text{sat}} + R_{\text{day}}) (c_i + K) / (c_i - \Gamma^*), \quad (1)$$

where $K = K_C (1 + O/K_O)$, K_C is the Michaelis–Menten coefficient of Rubisco for carboxylation (Pa), O is the partial pressure of oxygen (O_2) (Pa), K_O is the Michaelis–Menten coefficient of Rubisco for oxygenation (Pa) and Γ^* (Pa) is the CO_2 compensation point in the absence of mitochondrial respiration. When dark respiration was measured, we used this as an approximation to day respiration (i.e. we ignored the light inhibition of leaf respiration, which can lead to mitochondrial respiration in the light being reduced relative to respiration measured in the dark). If no respiration measurement was available, the following approximation was used:

$$V_{\text{cmax}} \approx A_{\text{sat}} / [(c_i - \Gamma^*) / (c_i + K) - b], \quad (2)$$

where $b = 0.015 \exp[-0.018 (T_{\text{leaf}} - 298.15)]$ and T_{leaf} is the leaf temperature in kelvin. Equation (2) is the corrected version of Equation (3) in De Kauwe et al. (2016), with an additional (slight) temperature dependence of b —which De Kauwe et al. (2016) set at a constant value of 0.015—based on the global analysis of leaf dark respiration data by Wang et al. (2020). (Note that the effect of alternative treatments of leaf respiration on estimated V_{cmax} is presumed to be minor, as leaf dark respiration is usually only about 5% of A_{sat} .) De Kauwe et al. (2016) showed that if R_{dark} estimated from V_{cmax} was used instead of R_{day} , the result was a small bias, and a reduction in R^2 from 0.98 to 0.95 when predicting V_{cmax} derived from traditional $A-c_i$ curve fitting, rather than from one-point estimated V_{cmax} . Reference values (at a common measurement temperature of 25°C) and temperature dependencies of K_C , K_O and Γ^* , and the temperature dependency of V_{cmax} , were derived from in vivo determinations in tobacco leaves (Bernacchi et al., 2001). Reference values were $K_C = 39.97$ Pa, $K_O = 27,480$ Pa and (at sea level) $\Gamma^* = 4.332$ Pa. The barometric formula (Davis et al., 2017) was used to estimate mean atmospheric pressure at site elevation (z), required to calculate c_i , O and Γ^* .

The primary data used to generate V_{cmax} values consisted of measurements carried out at different controlled cuvette temperatures. Therefore, they required conversion both to standard temperature (25°C: hence $V_{\text{cmax}25}$) to be comparable among sites and to local growth temperature ($V_{\text{cmax,gt}}$) for comparison with theoretical predictions. Conversion of observed V_{cmax} from measurement temperature (T_0) to target temperature (T_1) was performed using the Arrhenius equation:

$$V_{\text{cmax}}[T_1] = V_{\text{cmax}}[T_0] \exp[(\Delta H/R) (1/T_0 - 1/T_1)], \quad (3)$$

where ΔH is the activation energy of V_{cmax} (66,530 J mol⁻¹ following Bernacchi et al., 2001), R is the universal gas constant (8.314 J mol⁻¹ K⁻¹), and T_0 and T_1 are in kelvin.

2.2 | Independent theoretical predictions of V_{cmax}

According to the coordination hypothesis, the optimal value of V_{cmax} for plants acclimated to their current growth conditions ($V_{\text{cmax,gt}}$),

generally taken to be represented by averages during daylight hours over a period of a few weeks, can be approximated by the following formula (Togashi et al., 2018):

$$V_{\text{cmax,gt}} \approx \varphi_0 I_{\text{abs}} (c_i + K) / (c_i + 2\Gamma^*), \quad (4)$$

where φ_0 is the intrinsic quantum efficiency of photosynthesis (mol mol⁻¹), that is, the number of carbon atoms fixed per photon absorbed under non-photorespiratory conditions [saturating CO_2 and/or low O_2 ; Skillman 2008, and I_{abs} is the photosynthetic photon flux density (PPFD) absorbed by leaves ($\mu\text{mol m}^{-2} \text{s}^{-1}$)]. The choice of value for I_{abs} is important because predicted $V_{\text{cmax,gt}}$ is proportional to I_{abs} . Here I_{abs} is taken to be 80% of I_L , the estimated canopy-average PPFD, given by inversion of Beer's law as $I_L \approx -k I_0 f_v / \ln(1 - f_v)$ where f_v is the fractional vegetation cover (a function of leaf area index, derived from satellite data) and k is the extinction coefficient, for which we assign the commonly used generic value of 0.5 (Dong et al., 2017). This formula yields values $\approx k I_0$ for small f_v (thus accounting for the varying orientations of leaves, hence $k < 1$) and progressively declining values as f_v increases (accounting for decreasing light availability with increasing canopy depth). Thus, it takes account of the expectation that canopy-average V_{cmax} should be lower in communities with a higher leaf area index, due to greater shading.

The realized quantum efficiency, often denoted simply as φ , is the ratio of the assimilation rate (measured at low light intensity) to I_{abs} . This ratio depends on c_i . At current c_a , φ declines strongly with temperature due to increasing photorespiration (Skillman, 2008). In contrast, this decline does not affect the intrinsic quantum efficiency φ_0 , which is independent of photorespiration. In light-adapted leaves, nonetheless, φ_0 does respond to temperature variations—especially below about 15°C. We therefore applied an empirical expression for φ_0 (as a function of temperature T , in °C) from Bernacchi et al. (2003):

$$\varphi_0 = (0.352 + 0.021 T - 3.4 \times 10^{-4} T^2) / 8, \quad (5)$$

which takes a maximum value of 0.085 mol mol⁻¹ at 30.9°C. Values of c_i (Pa) in Equation (4) were obtained by the least-cost hypothesis:

$$c_i = \Gamma^* + (c_a - \Gamma^*) \xi / (\xi + \sqrt{D}), \text{ where} \quad (6a)$$

$$\xi = \sqrt{[\beta (K + \Gamma^*) / 1.6 \eta^*]}. \quad (6b)$$

The parameter ξ (in units of Pa^{1/2}) expresses the sensitivity of stomatal behaviour to vapour pressure deficit (D , in Pa). The scaling factor β is assigned the value 146, estimates under standard environmental conditions ($T = 25^\circ\text{C}$, $D = 1\text{ kPa}$, $z = 0$) based on a global analysis of leaf stable carbon isotope measurements (Stocker et al., 2020). η^* is the viscosity of water at growth temperature relative to its value at 25°C, which influences the cost of maintaining transpiration capacity (Prentice et al., 2014). The numerator of Equation (6b) increases with temperature while the denominator decreases, implying that c_i (all else equal) should increase with temperature. Both photosynthetic and

hydraulic effects must be considered to account for the full observed magnitude of the acclimated response of χ to temperature (Prentice et al., 2014). Annual values of the ambient CO₂ partial pressure (c_a , Pa) were derived from published measurements of the global average CO₂ mole fraction, converting these to pressure units to allow for the effect of elevation.

The theory outlined above yields site-specific canopy-average predicted values of $V_{c_{max,gt}}$. They were converted to standard temperature (25°C) by Equation (3), to test the possibility of using predicted $V_{c_{max,25}}$ values in a model for N_{area} .

2.3 | Independent theoretical predictions of optimal LMA

The leaf economics spectrum (Wright et al., 2004) can be explained by an extension of Kikuzawa's (1991) hypothesis that the relationship between LMA and leaf life span maximizes the lifetime-average net carbon gain. Wang et al. (2021) showed that optimal LMA according to this hypothesis was proportional to life span, and that the ratio between the two quantities varied as a function of climate. Multiple combinations of LMA and leaf lifespan (LL) in any one climate yield the same average net carbon gain. If leaf life span is unknown (as is commonly the case for evergreen species), the optimal site-mean LMA for evergreens can nonetheless be approximated (Wang et al., 2021) by:

$$\ln LMA_{ev} = 0.5 \ln I_L^* - 0.013 T + 0.25 \ln f + \beta_{\alpha, ev} \alpha + \beta_{0, ev}, \quad (7)$$

where the suffix 'ev' stands for evergreen, I_L^* is the daily (24 hours) total PPFD ($\text{mol m}^{-2} \text{d}^{-1}$) averaged over the thermal growing season (defined here as the period of the year with climatic average temperatures $>0^\circ\text{C}$), T is the mean growing-season annual daytime (daylight-hours) air temperature ($^\circ\text{C}$) estimated using Equation (9) below, f is the growing-season length as a fraction of the year, α is defined as the ratio of actual to equilibrium evapotranspiration (ranging from zero to its canonical maximum value of 1.26) as estimated by the SPLASH model (Davis et al., 2017), and $\beta_{\alpha, ev}$ (expressing the effect of hydroclimate on LMA for evergreen species) and $\beta_{0, ev}$ (a reference value of LMA for evergreen species) are empirical constants fitted to data. Equation (7) is based on the hypothesis that observed distributions of $\ln LMA$ in evergreen plants represent the intersection of a prior, bivariate lognormal distribution of LMA and leaf life span [estimated by Wang et al. (2021) from a global data set] with a line representing the predicted optimal relationship between LMA and leaf life span under a given set of environmental conditions. Deciduous plants behave differently, because their leaf life span is set by the length of the growing season while their leaf life cycle is 1 year. For deciduous species, the optimal site-mean LMA is approximated by Wang et al. (2021):

$$\ln LMA_{de} = \ln I_L^* - 0.052 T + \ln f + \beta_{\alpha, de} \alpha + \beta_{0, de} \quad (8)$$

where the suffix 'de' stands for deciduous, and $\beta_{\alpha, de}$ and $\beta_{0, de}$ are empirical constants fitted to data on deciduous species. By regressing observed $\ln LMA$ on the predictors (the variables on the right-hand sides of Equations (7) and (8)), we can estimate general values of the empirical constants. The fitted intercepts ($\beta_{0, ev}$, $\beta_{0, de}$) set the overall magnitude of predicted LMA for each phenological type but remain constant under different environmental conditions, allowing us to independently predict the patterns of variation in LMA among sites.

2.4 | Climate and soils data

Climatological mean values of daytime-average air temperature (T , $^\circ\text{C}$), vapour pressure deficit (D , Pa) and incident (top-of-canopy) PPFD (I_0 , $\mu\text{mol m}^{-2} \text{s}^{-1}$) during the thermal growing season were calculated for each site, based on monthly data (interpolated to daily timesteps) at 1 km resolution in the CHELSA dataset (Karger et al., 2017) and daily data at 0.5° resolution in the WATCH Forcing Data ERA Interim (WFDEI) bias-corrected climate reanalysis (Weedon et al., 2014) for 1980–2013, which is the longest common period for all climate datasets. The thermal growing season definition used here somewhat overestimates the actual growth period, for example, for temperate deciduous trees. We disregard this issue as this definition is widely used, and changes in the threshold temperature in our experience mainly affect the overall magnitude, but not the geographical pattern of variation, in T .

Mean daytime air temperature (T) is not provided in CHELSA or other global datasets that are based on direct spatial interpolation of weather-station observations. T was therefore estimated from daily temperature maxima and minima using the formula (Xu et al., 2021):

$$T = T_{max} \left(\frac{1}{2} + \frac{\sqrt{1-x^2}}{2\cos^{-1}x} \right) + T_{min} \left(\frac{1}{2} - \frac{\sqrt{1-x^2}}{2\cos^{-1}x} \right), \quad (9)$$

where T_{max} is the daily maximum air temperature (K), T_{min} is the daily minimum air temperature (K) and $x = -\tan \lambda \tan \delta$ where λ is latitude and δ is the daily solar declination, calculated using SPLASH (Davis et al., 2017). Equation (9) estimates the average air temperature during daylight hours, assuming that air temperature follows the same diurnal time course as potential solar radiation. T is a weighted average of T_{min} and T_{max} , approaching T_{max} as days become shorter, and approaching the daily mean temperature as days become longer. Although Equation (9) is an approximation (in reality maximum temperatures lag solar radiation by several hours, while minimum temperatures typically occur just before dawn), it is preferred here to mean daily temperature (commonly used in trait analyses) as it more closely corresponds to the conditions under which photosynthesis occurs.

I_0 was estimated from total daily incident shortwave radiation in WFDEI, assuming $2.04 \mu\text{mol J}^{-1}$ (photosynthetic photons per unit total short-wave radiation) and correcting for elevation by +2.7% per km (Davis et al., 2017). Canopy-average daytime PPFD (I_L) and the average daily (24 hours) PPFD (I_L^*) followed the approximation of

Dong et al. (2017) as described above, with f_v estimated from data in Zhu et al. (2013). I_L values were divided by daylength to provide daytime averages.

D was estimated from specific humidity data in WFDEI, with saturated vapour pressure calculated at the mean daytime temperature obtained from Equation (9) using the same equation as Stocker et al. (2020).

Soils data (% clay, pH and C:N ratio) were obtained from the ISRIC-WISE Derived Soil Properties dataset at 30 arc second resolution for the top 30 cm of topsoil (Batjes, 2016).

2.5 | Theoretical sensitivities of V_{cmax} and LMA to environmental variables

Partial regression slopes fitted to observations of a log-transformed response variable and several predictor variables can be numerically compared with the corresponding sensitivity coefficients derived from theory (e.g. Dong et al., 2017; Peng et al., 2021; Wang et al., 2017). These theoretical sensitivity coefficients can be obtained by taking partial derivatives of the log-transformed response variable with respect to each of the predictors. If the predictor also is log-transformed, the derivative is dimensionless. It can be understood as the logarithm of the percentage change induced in the response variable by a given percentage change in the predictor variable. For photosynthetic capacity:

1. The coordination hypothesis predicts a optimal value of V_{cmax} at growth temperature ($V_{\text{cmax,gt}}$) that increases in direct proportion to daytime-average light. In other words, the sensitivity coefficient ($\partial \ln V_{\text{cmax,gt}} / \partial \ln I_L$) for I_L is equal to unity.
2. Greater V_{cmax} is needed to achieve a given photosynthetic rate at higher leaf temperatures. The temperature dependencies of K and Γ^* are principally responsible for this, because larger K and Γ^* imply reduced photosynthesis as temperature increases. Therefore, the optimal $V_{\text{cmax,gt}}$, all else equal, increases with temperature. The formula for the sensitivity of optimal $V_{\text{cmax,gt}}$ to temperature (in K^{-1} , because log-transformation is usually inappropriate for temperatures) is a function of c_a and temperature that subsumes the temperature responses of several processes.
3. Higher D promotes a shift in the optimal leaf-level investment strategy towards higher photosynthetic capacity and lower water-transport capacity (Dong et al., 2020; Prentice et al., 2014; Wang et al., 2017). This shift results in a smaller optimal χ , and a higher V_{cmax} is required to achieve the same photosynthetic rate at a lower χ . The theoretical dimensionless sensitivity of optimal $V_{\text{cmax,gt}}$ to D is (Togashi et al., 2018):

$$\partial \ln V_{\text{cmax,gt}} / \partial \ln D = 0.5 c_a (1 - \Gamma^* / c_a) \chi (1 - \chi) [1 / (c_i + 2\Gamma^*) - 1 / (c_i + K)] \quad (10)$$

Theoretical sensitivities were evaluated under mean conditions ($T = 21^\circ\text{C}$, $D = 0.65\text{kPa}$, $z = 567$) with $c_a = 36.07\text{Pa}$ (equivalent to $380\mu\text{molmol}^{-1}$). The sensitivities of optimal $\ln V_{\text{cmax,gt}}$ to growth

temperature and $\ln D$ under standard conditions are 0.082K^{-1} and 0.056 , respectively. For optimal $\ln V_{\text{cmax25}}$, the sensitivity to growth temperature is under standard conditions is -0.0061K^{-1} . As these sensitivities vary with environmental conditions, we also evaluated them at each site, providing a range.

Sensitivities of optimal $\ln \text{LMA}$ to environmental variables (light, temperature and growing-season length) are implicit in Equations (7 and 8). The theory developed by Wang et al. (2021) does not make quantitative predictions for the sensitivities of optimal LMA to the moisture index α . However, it is expected that optimal LMA should decline with increasing α in both evergreen and deciduous plants, resulting in negative values of the coefficients $\beta_{\alpha\text{ev}}$ and $\beta_{\alpha\text{de}}$, as confirmed for observed LMA by Wang et al. (2021).

2.6 | Data analysis

All analyses and graphics were conducted in R (R Core Team, 2020). Ordinary least-squares linear (simple or multiple) regression was performed using the 'lm' function. Results of multiple regressions were visualized as partial residual plots using the VISREG package, in which for each predictor variable, the observed values of the response variable are adjusted so that all other predictors are held constant at their median values. The relative importance of different predictors was calculated using the Lindeman–Merenda–Gold (LMG) statistic. This measures the relative contribution made by a given predictor to increasing the R^2 of the multiple regression, averaged over all possible orders in which the predictors are introduced. (Note that LMG statistics sum to 100%, i.e. they indicate the relative importance of different variables' contributions to the final R^2 —not the absolute amount of variance that they explain.) LMG statistics were calculated using the 'lmg' function in the RELAIMPO package in R.

To test the hypothesis that global patterns of observed N_{area} reflect variations in observed LMA and V_{cmax25} , we regressed N_{area} on these two variables (Figures 1 and 2). Dong et al. (2017) showed that N-fixing species allocate more N per unit LMA than non-fixers; therefore, the factor 'N-fixer', and the interactions between 'N-fixer' and LMA, and between 'N-fixer' and V_{cmax25} , were added. This initial analysis was followed by a model selection step in which non-significant predictors were eliminated. Analyses were run for the entire dataset and separately for major functional groups (non-woody vs. woody species; and if woody, evergreen vs. deciduous species). N-fixers constituted 9.7% (298 species) of the full dataset, and similar fractions (8.6–13.0%) of each of the major functional groups. For completeness, alternative analyses were conducted in which the interaction between observed LMA and V_{cmax25} was also included (Table S2). A further analysis was conducted using observed leaf nitrogen per unit mass (N_{mass}) as the response variable, and the ratio $V_{\text{cmax25}}/\text{LMA}$ as the (single) predictor variable. Note that N_{mass} , V_{cmax25} and LMA are separately measured quantities. Thus, N_{mass} (unlike N_{area}) is statistically independent of LMA.

To test the coordination hypothesis for V_{cmax} , we regressed observed log-transformed $V_{\text{cmax,gt}}$ and V_{cmax25} on the three climatic

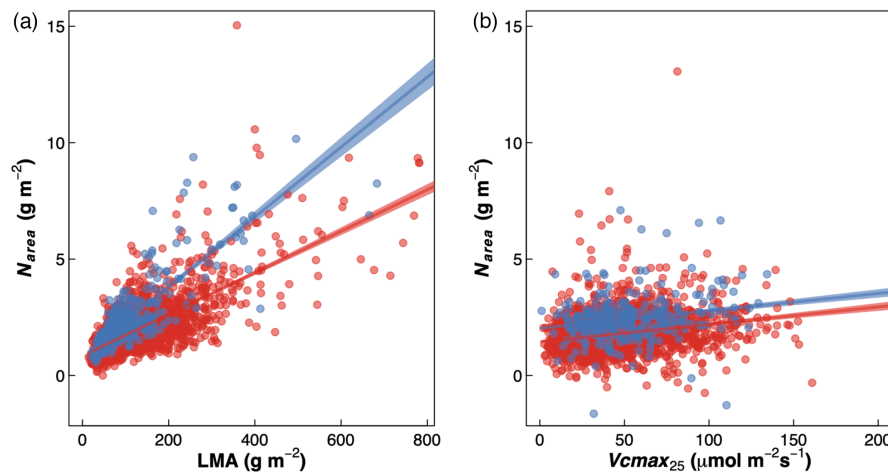
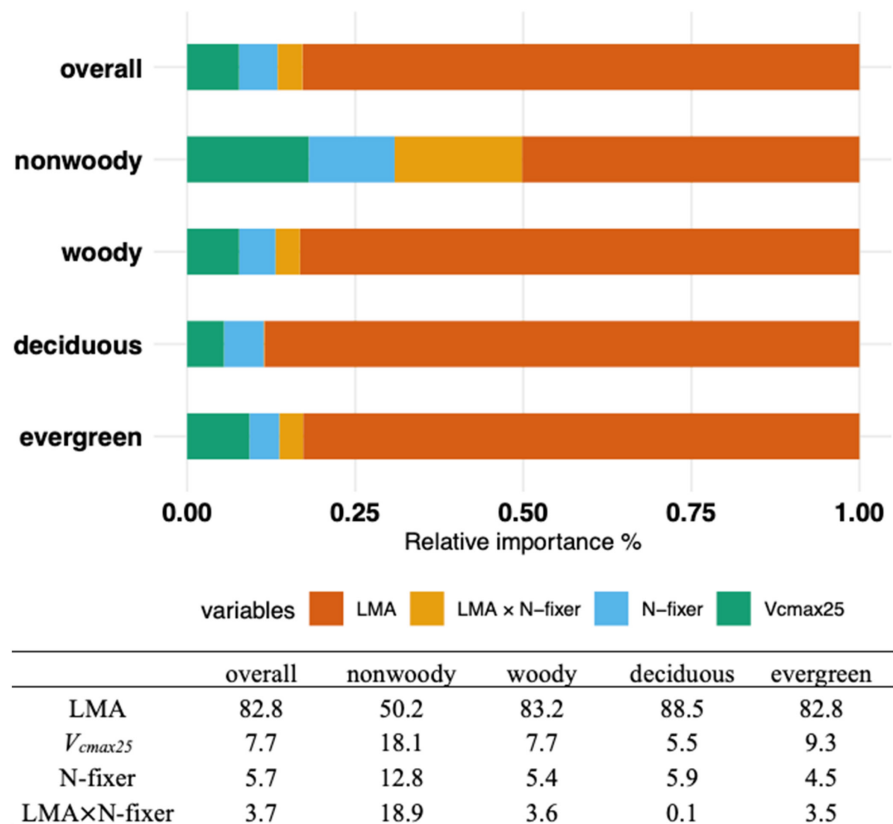


FIGURE 1 Partial residual plots of leaf nitrogen per unit area (N_{area} , g m^{-2}) as an additive function of (a) leaf mass per area (LMA, g m^{-2}) and (b) carboxylation capacity at 25°C ($V_{\text{cmax}25}$, $\mu\text{mol m}^{-2} \text{s}^{-1}$) across all species, based on the main regression equation of Table 1 ($N_{\text{area}} \sim \text{LMA} + V_{\text{cmax}25} + \text{LMA} \times N_{\text{fixer}}$). Each plot shows values of N_{area} corrected by holding the other variable constant at its median value. Nitrogen-fixers (N_{fixer}) are in blue, non-nitrogen-fixers in red. Coloured lines are partial regression lines; shading indicates 95% confidence bands.

FIGURE 2 Relative importance of each variable in explaining the variation of leaf nitrogen per unit area (N_{area} , g m^{-2}) across all species. Leaf mass per unit area (LMA, g m^{-2}), carboxylation capacity at 25°C ($V_{\text{cmax}25}$, $\mu\text{mol m}^{-2} \text{s}^{-1}$).



variables (T , $\ln I_L$ and $\ln D$) that are salient predictors of V_{cmax} according to this hypothesis (Peng et al., 2021; Smith et al., 2019; Figure 3).

To test the optimality hypothesis for LMA, we regressed observed log-transformed LMA on the four climatic variables (T , $\ln I_L$, $\ln \alpha$ and $\ln f$) that are salient predictors according to the extended Kikuzawa hypothesis (Wang et al., 2021; Wright et al., 2004; Figure 4). Evergreen and deciduous woody plants were analysed separately. We also analysed observed LMA of non-woody plants,

provisionally assigning species from cold-winter climates ($f < 1$; 'cold' non-woody plants) to the deciduous group, and species from tropical/sub-tropical climates ($f = 1$; 'warm' non-woody plants) to the evergreen group.

To assess the potential for observed N_{area} to be predicted from climate, we compared observed values of N_{area} with predicted values of N_{area} based on independently calculated optimal LMA and optimal $V_{\text{cmax}25}$ (Figure 5).

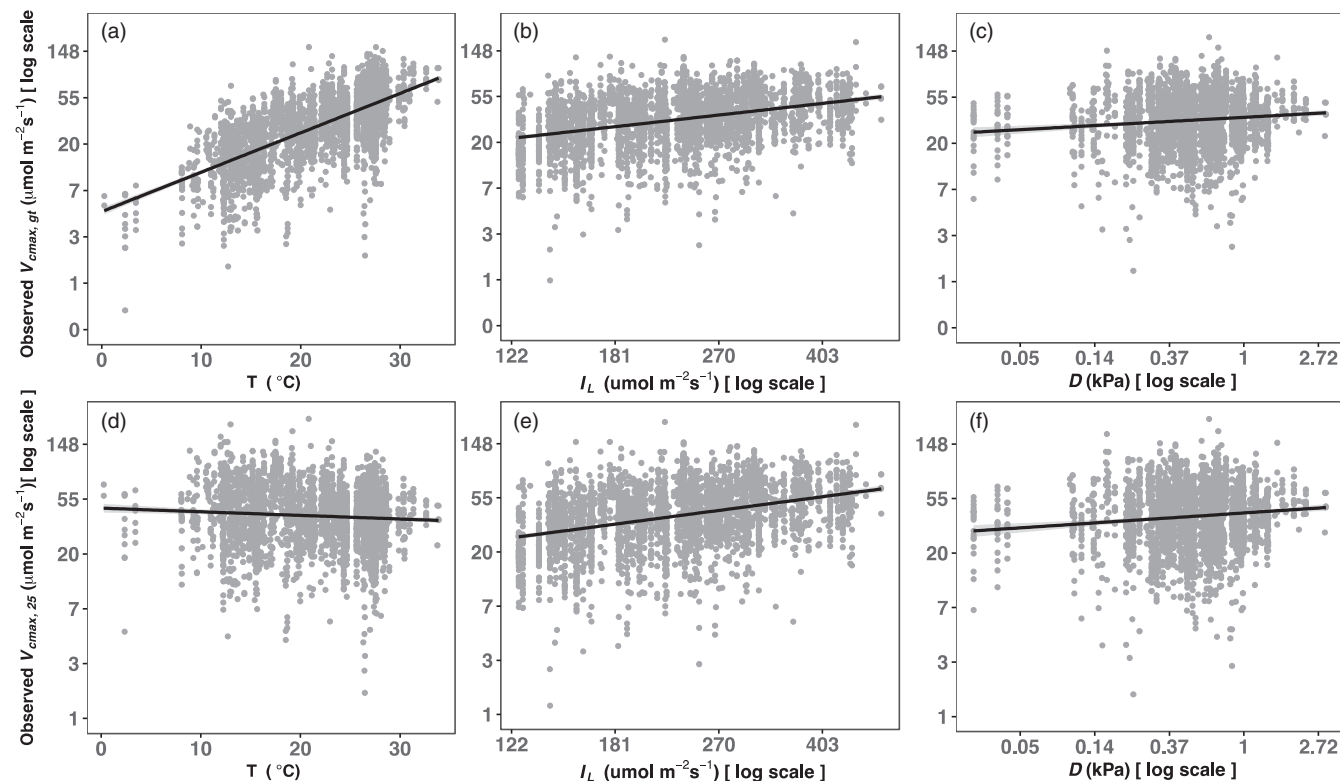


FIGURE 3 Partial residual plots of log-transformed carboxylation capacity at growth temperature ($V_{cmax,gt}$, $\mu\text{mol m}^{-2} \text{s}^{-1}$) (a–c) and at 25°C (d–f) versus (a, d) growing-season daytime mean temperature (T , °C), (b, e) log-transformed growing-season daytime mean photosynthetic photon flux density (I_L , $\mu\text{mol m}^{-2} \text{s}^{-1}$), and (c, f) growing-season daytime vapour pressure deficit (D , kPa) across all species. Black lines are partial regression lines; grey shading indicates 95% confidence bands.

To assess the extent to which soil properties modify the relationships of leaf traits to climate, we analysed the bias of predicted optimal V_{cmax25} , predicted optimal LMA and the estimate of N_{area} obtained from these quantities, by multiple regression using % clay, pH and C:N ratio as predictors. Model bias was quantified as the log-ratio of predicted to observed values.

3 | RESULTS

3.1 | N_{area} as a function of other plant traits

A multiple linear regression with observed V_{cmax25} , LMA, the factor 'N-fixer' and the interaction of LMA and 'N-fixer' as predictors accounted for 60% of variation in N_{area} over all species (all predictors significant at $p < 0.001$: Table 1). The interaction of V_{cmax25} and the factor 'N-fixer' was non-significant, and therefore removed. N-fixers however showed steeper observed N_{area} -LMA slopes than non-fixers (Figure 1a) due to a significant interaction between 'N-fixer' and LMA (Table 1). The fitted positive relationships of observed N_{area} to both observed LMA (Figure 1a) and V_{cmax25} (Figure 1b) were highly significant ($p < 0.001$), but the explanatory power of the relationship to LMA was substantially larger than that for V_{cmax25} (Figure 2).

Woody species comprised about 90% of the dataset (2806/3093 species); hence, analyses considering woody species alone yielded similar results to the all-species analysis (Table 1; Figure 2). N-fixers

allocated more N per unit LMA than non-fixers, as shown by the significant interaction between LMA and 'N-fixer'. When woody species were separated into phenological types, V_{cmax25} explained a higher proportion of N_{area} variation in evergreen than in deciduous species (Table 1). Among deciduous species, N-fixers had higher N_{area} values than evergreen species, but the interaction of 'N-fixer' with LMA was non-significant (Table 1). LMA was by far the most important predictor (>80% of explained variance) of N_{area} for woody species, irrespective of whether they were evergreen or deciduous (Figure 2). Even among non-woody species, encompassing a smaller range of variation in LMA than woody species, LMA was the most important predictor (>50%) of N_{area} . In the overall analysis and the analysis of subsets, explanatory power (R^2) and RMSE were close in out-of-sample tests where a randomly chosen 25% of the data were withheld and used for evaluation (Table S4).

Statistically significant negative interaction effects between observed V_{cmax25} and LMA were also shown (Table S2: except in deciduous woody plants), indicating that the effect of V_{cmax25} on leaf N is less in high-LMA leaves. The cause of this interaction is unclear. However, the inclusion of these interactions caused only very minor changes in the other regression coefficients, did not substantially increase explained variance and contributed less than 1% in terms of relative importance.

A linear regression across all species relating observed N_{mass} to the observed ratio V_{cmax25}/LMA yielded the equation $N_{mass} = 0.014 (\pm 0.0002) + 0.011 (\pm 0.0003) V_{cmax25}/LMA$, accounting for 31%

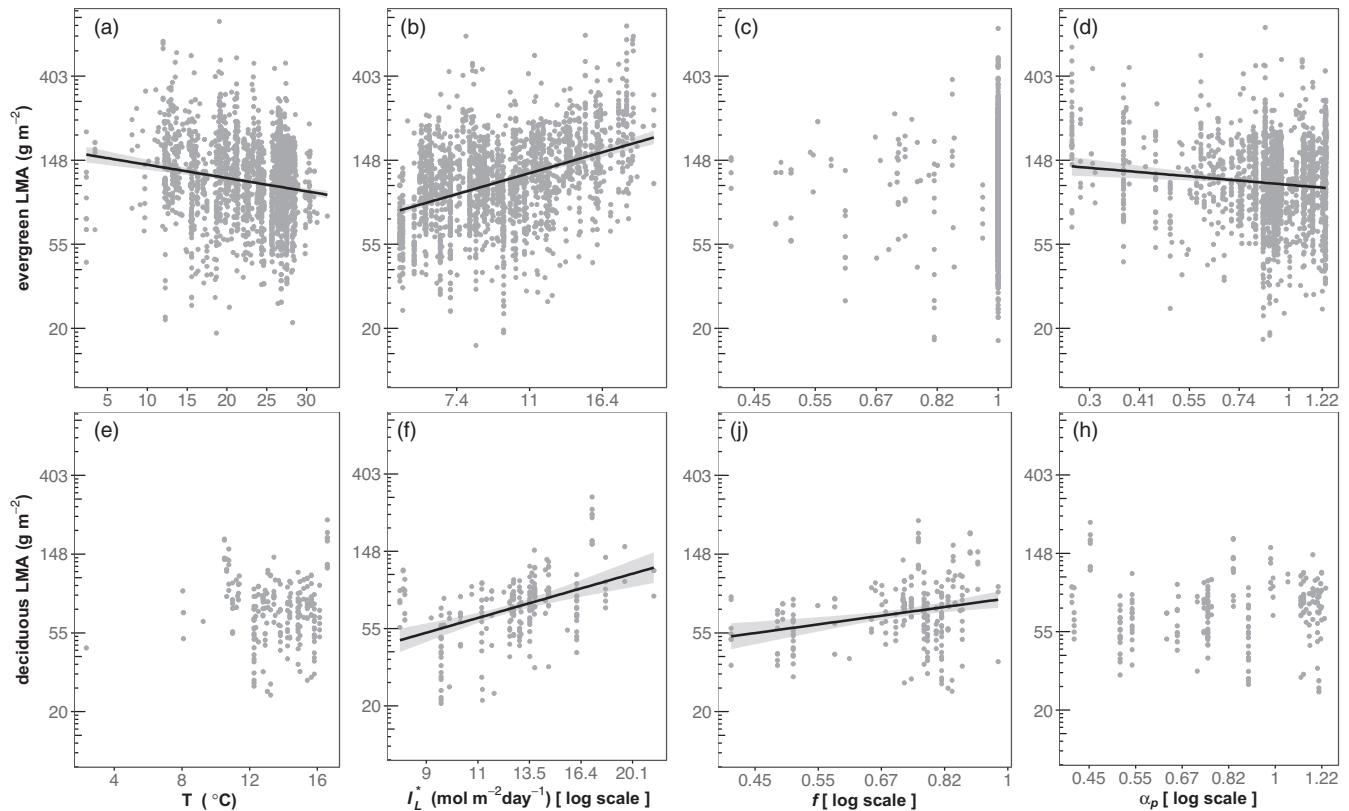


FIGURE 4 Partial residual plots of log-transformed leaf mass per unit area (LMA, g m^{-2}) versus growing-season daytime mean temperature (T , $^{\circ}\text{C}$), log-transformed growing-season mean daily total photosynthetic photon flux density (I_L^* , $\text{mol m}^{-2} \text{day}^{-1}$), growing-season length as a fraction of the year (f , day day^{-1}), and actual/equilibrium evapotranspiration (α , dimensionless) in evergreen (a–d) and deciduous (e–h) woody plants. Black lines are partial regression lines; grey shading indicates 95% confidence bands.

($p < 0.001$) of the variance in N_{mass} (Figure S2). The relative importance of $V_{\text{cmax}25}$ and LMA was assessed by comparing this result with regressions against $V_{\text{cmax}25}$ and LMA alone, yielding LMG statistics of 80% for LMA and 20% for $V_{\text{cmax}25}$. The simple bivariate relationships of both observed N_{area} and N_{mass} to observed LMA and $V_{\text{cmax}25}$ (Figure S3) were also shown for completeness.

Our analysis thus provides global-scale support for the hypothesis of Dong et al. (2017) that leaf N can be approximated as the sum of two components, one proportional to observed $V_{\text{cmax}25}$ (based on gas-exchange measurements) and the other to observed LMA. It also underlines the importance of LMA, when considering all types of plants and climates, as a predictor of total leaf N.

3.2 | V_{cmax} as a function of climate

We estimated the climatic controls on observed $V_{\text{cmax,gt}}$ using multiple regression. Significant positive relationships were found for observed log-transformed $V_{\text{cmax,gt}}$ with respect to growing-season values of log-transformed PFD ($\ln I_L^*$), temperature (T) and log-transformed D ($\ln D$; Table 2; Figure 3). These three variables together explained 48% of the variance in observed $V_{\text{cmax,gt}}$ (Table 2). The fitted slope for $\ln I_L^*$ (0.64, 95% confidence interval 0.57 to 0.71)

was somewhat smaller than the theoretical value of 1 (Table 2). The fitted slope for T (0.085, 95% confidence interval 0.081–0.089 K^{-1}) lay within the predicted range (0.06–0.12 K^{-1}). The fitted slope for $\ln D$ (0.089, 95% confidence interval 0.055–0.124) straddled the top of the predicted range (0.00–0.09; Table 2; Figure 3).

We also estimated the climatic controls on observed $V_{\text{cmax}25}$ (Table 2; Figure 3). The same three variables together explained 18% of the variance in $V_{\text{cmax}25}$. A significant negative partial relationship was found for observed $V_{\text{cmax}25}$ with respect to growing-season temperature (Table S8) with a slope (-0.007 , 95% confidence interval -0.010 to -0.003K^{-1}) not significantly different from the predicted slope evaluated under mean conditions (-0.006K^{-1}). The partial relationships with $\ln I_L^*$ and $\ln D$ were closely similar to those for observed $V_{\text{cmax,gt}}$, as expected.

Our analysis thus further strengthens the support for the hypothesis of Dong et al. (2017), Smith et al. (2019) and others that V_{cmax} optimally adjusts to the growth environment. The observed negative response of $V_{\text{cmax}25}$ (i.e. after the enzyme-kinetic response of V_{cmax} to temperature has been removed) to growth temperature is consistent with experimental findings (Scafero et al., 2017), as well as theoretical expectations. This relationship is weaker than the positive response of observed $V_{\text{cmax,gt}}$ to growth temperature, but significant nonetheless.

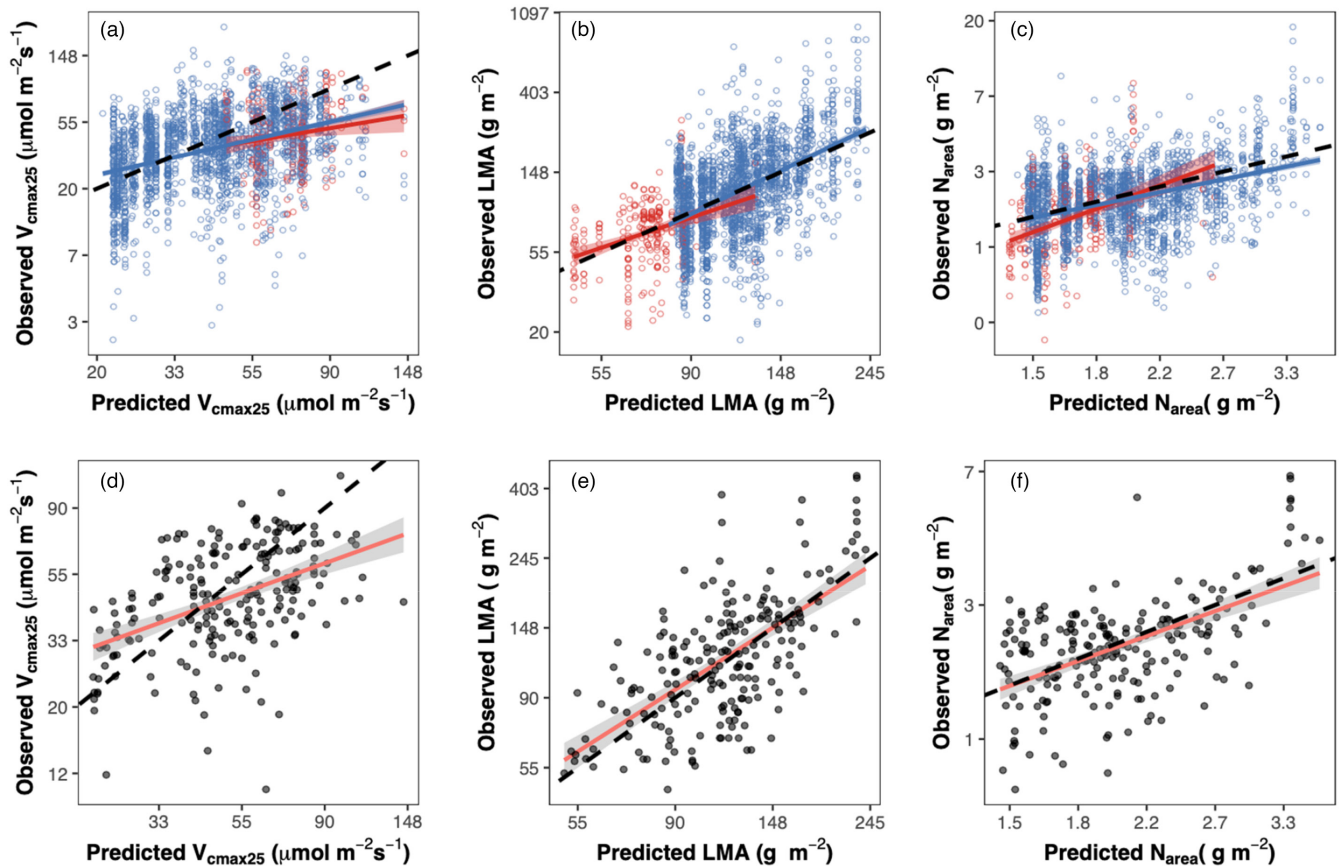


FIGURE 5 Predicted versus observed all-species (a–c) and site-mean (d–f) carboxylation capacity at 25°C (V_{cmax25} , $\mu\text{mol m}^{-2} \text{s}^{-1}$), leaf mass per unit area (LMA, g m^{-2}) and leaf nitrogen per unit area (N_{area} , g m^{-2}). The dashed lines are the 1:1 lines. Coloured lines are regression lines; shading indicates 95% confidence bands. Blue: evergreen species, red: deciduous species.

N_{area}	Overall	Non-Woody	Woody	Deciduous	Evergreen
LMA	0.009* (0.0002)	0.007* (0.0006)	0.009* (0.0002)	0.014* (0.0005)	0.008* (0.0002)
V_{cmax25}	0.007* (0.001)	0.010* (0.001)	0.007* (0.001)	0.006* (0.001)	0.006* (0.001)
N-fixer	-0.045 (0.159)	-1.134* (0.233)	-0.059 (0.174)	0.444* (0.243)	-0.146 (0.281)
LMA × N-fixer	0.006* (0.002)	0.026* (0.004)	0.006* (0.002)	0.001 (0.003)	0.006* (0.002)
Intercept	0.535* (0.045)	0.437* (0.072)	0.557* (0.049)	0.267* (0.091)	0.596* (0.056)
df	3093	250	2806	690	2016
Adjusted R^2	60%	73%	59%	65%	58%
RMSE	0.74	0.5	0.75	0.64	0.75

TABLE 1 Linear regression coefficients and (standard errors) for leaf nitrogen per unit area (N_{area} , g m^{-2}) as a function of leaf mass per area (LMA, g m^{-2}), carboxylation capacity at 25°C (V_{cmax25} , $\mu\text{mol m}^{-2} \text{s}^{-1}$), and the interaction term LMA × N-fixer, for all species ('main') and for each functional group. *Means $p < 0.01$; all other coefficients were non-significant ($p > 0.05$)

3.3 | LMA as a function of climate

For evergreens, in line with theoretical predictions, observed LMA was significantly negatively related to temperature (T , $p < 0.001$) and the log-transformed index of plant-available moisture ($\ln \alpha$,

$p < 0.001$), and significantly positively related to log-transformed PPFD ($\ln I_L^*$, $p < 0.001$; Table 3; Figure 4). Observed LMA was also weakly related to growing-season length ($\ln f$, $p = 0.08$). The four variables together explained 25% of the variance in observed evergreen LMA (Table 3; Figure 4). The fitted slopes were not

TABLE 2 Linear regression coefficients for log-transformed carboxylation capacity at growth temperature ($V_{\text{cmax,gt}}$, $\mu\text{mol m}^{-2} \text{s}^{-1}$) and at 25°C ($V_{\text{cmax}25}$, $\mu\text{mol m}^{-2} \text{s}^{-1}$) as a function of growing-season mean daytime temperature (T , °C), and log-transformed daytime growing-season mean photosynthetic photon flux density (I_L , $\mu\text{mol m}^{-2} \text{s}^{-1}$) and daytime vapour pressure deficit (D , kPa). Relative importance is indicated by the Lindeman–Merenda–Gold (LMG) statistic, which quantifies the relative contribution of each variable to the final R^2

Predictor	Fitted slope	95% confidence intervals	Range of predicted slopes	Relative importance (%)	p	R^2
At growth temperature						
$\ln I_L$	0.636	0.565, 0.707	1	8	<0.001	48%
T	0.085	0.081, 0.089	0.06, 0.12	78	<0.001	
$\ln D$	0.089	0.055, 0.124	0.00, 0.09	14	<0.001	
At 25°C						
$\ln I_L$	0.633	0.562, 0.704	1	71	<0.001	18%
T	-0.007	-0.010, -0.003	-0.048, 0.017	8	<0.001	
$\ln D$	0.091	0.056, 0.126	0, 0.090	21	<0.001	

TABLE 3 Linear regression coefficients for leaf mass per area as a function of growing-season mean daytime temperature (T , °C) and log-transformed growing-season mean daily photosynthetic photon flux density (I_L^* , $\text{mol m}^{-2} \text{day}^{-1}$), growing-season length as a fraction of the year (f), and actual/equilibrium evapotranspiration (α , dimensionless) in evergreen and deciduous woody plants. Theoretical values are from Table S2 in Wang et al. (2021)

	Variable	Theoretical value	Fitted value	95% confidence intervals	p -value	R^2	df
Evergreen	$\ln I_L^*$	0.50	0.62	0.54, 0.71	<0.001	25%	2009
	T	-0.013	-0.016	-0.02, -0.01	<0.001		
	$\ln f$	0.25	(0.22)	-0.03, 0.48	0.08		
	$\ln \alpha$	n/a	-0.17	-0.26, -0.08	<0.001		
	Intercept	n/a	3.72	3.50, 3.95	<0.001		
Deciduous	$\ln I_L^*$	1	0.95	0.62, 1.29	<0.001	18%	235
	T	-0.052	(-0.0003)	(-0.03, 0.03)	0.98		
	$\ln f$	1	0.55	0.26, 0.84	<0.001		
	$\ln \alpha$	n/a	(0.06)	(-0.1, 0.22)	0.43		
	Intercept	n/a	2.00	1.34, 2.68	<0.001		

statistically distinguishable from the theoretical slopes as given by Wang et al. (2021).

For deciduous species, also in line with theoretical predictions, observed LMA was significantly positively related to $\ln I_L$ and $\ln f$ (Table 3; Figure 4). The four variables together explained 18% of the variance in observed deciduous LMA. The fitted slope was not significantly different from the theoretical slope for $\ln I_L$ (0.95, 95% confidence interval 0.62–1.24, vs. 1; Wang et al., 2021), but the fitted slope for $\ln f$ was shallower than the theoretical slope (0.55, 95% confidence interval 0.26–0.84, vs. 1). No significant relationships were shown for T or $\ln \alpha$, perhaps because of the small sample size and/or the relatively narrow range of growth temperatures for deciduous species in this dataset.

Table S3 and Figure S4 showed corresponding results for non-woody species, based on smaller datasets. Observed LMA was shown to increase with I_L in both groups ('cold' and 'warm'), albeit more steeply than predicted in the 'cold' group, and to increase in proportion to f in the 'cold' group. The 'cold' group also showed a decline of observed LMA with increasing temperature that is consistent with the theoretical prediction for deciduous species.

Our analysis thus supports the hypothesis of Wang et al. (2021) that large-scale patterns in evergreen LMA follow a predictable pattern, whereby local distributions of LMA are determined by the intersection of a prior distribution of LMA and LL and a climatically determined coefficient of proportionality between LMA and LL. It is also consistent with the predictions of Wang et al. (2021) for LMA in deciduous species, although not all predictors of deciduous LMA showed significant effects.

3.4 | Predicted versus observed leaf traits

Our theoretical framework makes a single prediction of optimal $V_{\text{cmax,gt}}$ per site. We therefore considered the controls on site-mean trait values (excluding sites represented by less than three species). Good agreement was shown between site-mean values of observed $V_{\text{cmax,gt}}$ and predicted optimal $V_{\text{cmax,gt}}$ for the 217 study sites, with $R^2 = 67\%$ and a slope not statistically distinguishable from unity (Figure S5). Figure 5 compared observed values of $V_{\text{cmax}25}$, LMA and N_{area} with corresponding values of predicted

TABLE 4 Linear regression coefficients for the bias (log-ratio of predicted to observed values, dimensionless) of the theoretical models for $V_{\text{cmax}25}$, LMA and N_{area} as a function of soil properties

	Predictor	Fitted slope	<i>p</i>	<i>R</i> ²
$V_{\text{cmax}25}$ bias	C:N	(0.03)	0.10	10%
	pH	(0.08)	0.06	
	% clay	-0.01	0.003	
LMA bias	C:N	(-0.01)	0.32	3%
	pH	(0.01)	0.83	
	% clay	0.01	0.04	
N_{area} bias	C:N	0.03	0.02	3%
	pH	(0.02)	0.66	
	% clay	(0.001)	0.47	

optimal $V_{\text{cmax}25}$ and LMA, and N_{area} as estimated from these two quantities for both species and site-means. In site-mean analyses, the optimality-based predictions explained 21% of the variance in observed $V_{\text{cmax}25}$ (Figure 5d) and 43% of the variance in observed LMA (Figure 5e). The corresponding figure for observed N_{area} was 31% (Figure 5f). Analyses for all species (Figure 5a–c) accounted for smaller fractions of variance, as expected because environmental inputs are constant for each site. Slopes of predicted versus observed values were indistinguishable from unity except for $V_{\text{cmax}25}$, which showed greater scatter than the other traits, and a lower slope. Scatter remaining in the site-mean analyses could have many causes, as the predictions involved numerous approximations—for example, in the estimation of effective growing-season length, daytime temperature and canopy-average light.

3.5 | Model bias in relation to soil properties

We assessed the effects of soil properties on $V_{\text{cmax}25}$, LMA and N_{area} by analysing the residuals from the predictions of the optimality model. Table 4 and Figure S6 presented partial relationships of model bias to soil properties in a multiple regression. Percent clay showed a negative relationship with the model bias of $V_{\text{cmax}25}$ (i.e. $V_{\text{cmax}25}$ was underestimated on clay-rich soils). On the other hand, LMA was overestimated on clay rich-soils, leading to no net bias for predicted N_{area} . N_{area} bias showed a weak positive relationship with soil C:N ratio, that is, N_{area} was overestimated on more organic soils.

4 | DISCUSSION

4.1 | Components of leaf nitrogen

We fitted a model for N_{area} with just two components. These might be interpreted as structural (i.e. cell-wall) N and metabolic (primarily Rubisco) N, but the full picture is more complex (Onoda et al., 2017; Osnas et al., 2013). The component proportional to

LMA must also include metabolic N required for the functioning of all leaf cells, including nucleic acids and defence compounds (Dong et al., 2017). The greater allocation of N to the LMA component in N-fixers may reflect a greater reliance on N-containing defence compounds (as opposed to physical, carbon-based defences). The component proportional to $V_{\text{cmax}25}$ must also include N linked to multiple functions, including respiration, that are coordinated with carboxylation (Wang et al., 2020). In any case, both components were required to explain the global pattern of variation in leaf N. Our results highlight the importance of LMA in predicting leaf N, especially in woody plants, regardless of whether it is expressed as N_{area} (increasing with LMA, as more leaf tissue inevitably means more N) or N_{mass} (decreasing with LMA, as low-LMA leaves contain a larger fraction of N-rich photosynthetic cells). The percentage of variance explained by the all-species regression equation for observed N_{area} (60%) could be inflated because N_{area} was not statistically independent of observed LMA (being calculated from observed N_{mass} and LMA). However, the corresponding equation relating observed N_{mass} to the observed ratio $V_{\text{cmax}25}$ /LMA explained 31% of the variation in observed N_{mass} , indicating that the predictability of leaf N is not a statistical artefact.

Several caveats to our analysis are in order. The apparent LMA-related contribution to N_{area} could be inflated by the assumption of infinite mesophyll conductance (g_m), implicit in the use of $A-c_i$ (rather than $A-c_c$) curves to estimate V_{cmax} . This could cause underestimation of V_{cmax} , especially in high-LMA leaves, which typically have low g_m (Flexas et al., 2013). Woody plant leaves may contain a larger fraction of inactive Rubisco compared to herbaceous plant leaves, due to sink limitation of photosynthesis (Stitt & Schulze, 1994; Warren & Adams, 2001). The LMA-related contribution, for woody plants especially, could thus partly be 'photosynthetic' N that is not reflected in field measurements of photosynthesis. Clarification of these points awaits further physiological research on leaf N partitioning. A final caveat is that V_{cmax} is not necessarily measured at its peak value. The theory to predict optimal LMA depends on the observed decline in photosynthetic capacity over time, implying that observed V_{cmax} values may be smaller than calculated optimal values. This tendency is probably minimized by standard sampling procedures (prioritizing outer-canopy leaves, and usually sampling in the middle part of the growing season) but inevitably introduces uncertainty, especially for deciduous species, whose photosynthetic capacity declines relatively rapidly during the season (Wang et al., 2021).

The dependency of observed total leaf N on observed LMA and $V_{\text{cmax}25}$ is, nonetheless, a robust empirical relationship. Indirect support for its mechanistic basis comes from the values of the coefficients. Analysis by Smith and Keenan (2020) indicated a Rubisco contribution of 0.004 g for each $\mu\text{mol s}^{-1}$ of $V_{\text{cmax}25}$, and a cytochrome *f* contribution of 0.0008 g for each $\mu\text{mol s}^{-1}$ of electron transport capacity ($J_{\text{max}25}$). Assuming a ratio of ≈ 2 between $J_{\text{max}25}$ and $V_{\text{cmax}25}$, these figures imply a total photosynthetic contribution of around 0.006 g leaf N per $\mu\text{mol s}^{-1}$ of photosynthetic capacity, similar to the coefficient of 0.007 (95% confidence

intervals 0.006–0.009) from our main analysis (Table 1). The coefficient for LMA (0.009) implies a realistic 'floor' of just under 1% N by mass.

4.2 | Acclimated responses of photosynthetic capacity

Our analysis supports the hypothesis that photosynthetic capacities are generally close to optimality based on the light, temperature and D conditions in which the plants are growing (Smith et al., 2019). The response of optimal $V_{\text{cmax,gt}}$ to growth temperature is an increase and required to compensate for increased photorespiration (Dong et al., 2017; Smith et al., 2019). This must not be confused with the instantaneous, enzyme-kinetic response of V_{cmax} to temperature, which is significantly steeper (Wang et al., 2020). Indeed, field-measured V_{cmax25} shows a compensating decline as growth temperature increases (Togashi et al., 2018). This is consistent with the coordination hypothesis because less Rubisco is required (Scafero et al., 2017) to produce the same catalytic effect at a higher temperature—and this effect is stronger than the response of optimal $V_{\text{cmax,gt}}$ to growth temperature (Dong et al., 2017). The instantaneous response operates over seconds to minutes. The time-scale of acclimation is not firmly established, but it is certainly slower. One recent study estimated a median response time of 1.5 months for the acclimation of $V_{\text{cmax,gt}}$ (Jiang et al., 2020). Acclimation could show different temporal characteristics in evergreen versus deciduous canopies. Current knowledge on this topic is limited because of the paucity of studies involving repeated measurements of photosynthetic traits within a single growing season. We assume, however, that in deciduous canopies especially, most measurements will have been made near the seasonal peak of photosynthetic capacity.

Empirical slopes of observed $V_{\text{cmax,gt}}$ with respect to PPFD, temperature and D in this study had the same signs as predicted relationships for predicted $V_{\text{cmax,gt}}$. The empirical relationship for PPFD, however, was shallower than the theoretical (proportional) response. In experiments on single species, although photosynthetic capacity was shown to respond steeply to the daily light integral, the response fell short of a 1:1 relationship (Poorter et al., 2019). This might be due to additional costs of producing high-capacity leaves that are not accounted for in our theory.

4.3 | Causes of the $V_{\text{cmax}}-N_{\text{area}}$ relationship

The observed positive correlation between V_{cmax25} and N_{area} could originate in any of three ways: (1) leaf N may determine V_{cmax25} ; (2) V_{cmax25} may determine leaf N; and (3) both leaf N and V_{cmax25} may be regulated by some other factor(s) (Field & Mooney, 1986). These possibilities are not mutually exclusive.

The first explanation (Walker et al., 2014)—that leaf N determines V_{cmax25} —is implicit in those models in which N uptake from

soils, and a fixed carbon allocation coefficient for foliage, combine to determine N_{area} and thence leaf-level V_{cmax25} . This can be considered as a 'supply side' interpretation of the relationship between leaf N and V_{cmax25} .

However, the second explanation—that the metabolic component of leaf N is a consequence (rather than a cause) of V_{cmax25} —is equally viable (Evans, 1989). Plants can alter carbon allocation between leaves and roots, allowing leaves to balance nutrient supply and demand. Allocation to roots is expected to be optimized such that the opportunity cost of photosynthesis foregone due to reduced canopy leaf area is matched by increasing access to nutrients (Givnish, 1987; Maire et al., 2013; Osone et al., 2008). Low soil N availability should then result in reduced carbon allocation to leaves and increased allocation below-ground—to roots, and possibly export to the rhizosphere (Fontaine et al., 2011). Moreover, there is no contradiction between this 'demand side' interpretation of the relationship between leaf N and V_{cmax25} and the widely observed 'N limitation' of primary production (i.e. N fertilization increases plant growth) under either ambient or elevated CO_2 . Plants subject to restricted N supply commonly respond by producing fewer leaves (rather than the same number of suboptimal ones), resulting in reduced primary production (Brix & Ebell, 1969). The fact that N-fixers do not show consistently higher rates of photosynthesis than other species (Adams et al., 2016), despite having access to an additional N source, further supports the hypothesis that leaf N is not generally limited by N supply. It remains to be determined, however, why N-fixers should allocate more N to LMA (Figure 1), given the high energetic costs of symbiotic N fixation.

Our results also provide some support for the third explanation. Some environmental characteristics (including aridity and high light intensity) promote both large LMA and high V_{cmax} , and could therefore contribute to a positive correlation between V_{cmax25} and N_{area} .

4.4 | The role of soil properties

Optimality theory predicts that soil conditions should influence trait values by altering the costs of nutrient acquisition, which are presumed to be greater on less fertile soils (Givnish, 1979; Paillassa et al., 2020). A theoretical model based on climate alone underestimated V_{cmax25} on clay-rich soils. This finding could be related to the phosphorus (P) content of clay minerals, and the influence of soil P availability on leaf P content and photosynthetic capacity (Bloomfield et al., 2014). Our model also overestimated LMA on clay-rich soils, which could relate to the influence of soil P availability on plant carbon uptake (Yang et al., 2021). These biases offset one another, resulting in no significant relationship of model bias for N_{area} to soil clay content. Effects of pH on leaf traits have been found previously, for example, by Maire et al. (2015) and Dong et al. (2020). The present analysis showed no significant effect of soil pH on model bias for the three traits, when the other soil properties were included. However, we found a significant relationship between the model bias for N_{area} and soil C:N ratio,

indicating that N_{area} on organic soils falls below values predicted by climate alone (Table 4).

These relatively small effects of soil factors on model bias should be viewed with caution. Inferences about the contribution of soils to the determination of leaf traits based on large observational datasets are constrained by the general lack of direct site measurements of soil properties. This situation is problematic because soil variation is typically abrupt, so any gridded dataset can be an inaccurate guide to site-specific soil properties. Nonetheless, the significant effects shown for % clay on both $V_{\text{cmax}25}$ and LMA, and for C:N ratio on N_{area} , suggest that a more complete analysis would likely reveal the effects of soil fertility factors modulating the optimal leaf-trait responses to the physical environment of growth.

4.5 | What do N addition experiments show?

Experimental N addition has sometimes (but not universally) been shown to increase both leaf N content and leaf-level photosynthesis—indicating that soil N availability can play a role in determining these quantities. Recent meta-analyses of N addition experiments (Firn et al., 2020; Li et al., 2020; Liang et al., 2020) have thrown some light on the apparent contradiction of leaf-level optimality versus soil N-availability controls on leaf N.

1. Firn et al. (2020), analysing data from the worldwide NutNet experiment, showed increases in N_{mass} resulting from experimental N addition. LMA did not change, implying that these increases were also reflected in N_{area} . However, the range of variation in leaf N content across sites was much larger than this experimental effect, indicating dominant control of global-scale variation in leaf N by other environmental factors (see e.g. Figure 4 in Firn et al., 2020).
2. Liang et al. (2020) showed that experimental N addition (this meta-analysis included data from experiments with many different level of N addition) increased leaf-level photosynthetic rates on average by 13% and N_{area} by 18%, while leaf area index (LAI) increased by 24% and total leaf biomass by 47%. This finding suggests that added N is preferentially allocated to produce new tissues.
3. Both Liang et al. (2020) and Li et al. (2020) found that leaf-level N increased in response to N fertilization are transient, vanishing after 5–10 years. Short-term responses to added N may thus not accurately predict plants' behaviour under natural conditions.

From an optimality perspective, it is also important to note that fertilization experiments supply additional N without cost to the plant. Under natural conditions, the energetic costs of N acquisition have to be set against the photosynthetic benefits. This trade-off may limit plants' investment in N acquisition. In addition, the responses of an extant ecosystem to experimental N addition may not accurately represent the long-term adjustment of site-mean leaf N

through competition among species differing in LMA, a distinction noted by Osnas et al. (2018).

Current understanding of how N availability influences photosynthesis and leaf N is thus incomplete. Inferences from large-scale analyses of uncontrolled field data are constrained by the lack of in situ soil measurements, and the lack of independence among different dimensions of soil and climate variation. How nutrient supplies influence the photosynthetic versus structural components of leaf N may be better illuminated by controlled-environment experiments, but the interpretation of experimental results must take into consideration the energetic costs of N uptake from soil by plants growing under natural conditions, and it must be recognized that global patterns of site-mean leaf N are likely to be influenced as much by species distributions and interspecies competition as by acclimation at the level of individual leaves and plants.

4.6 | Implications for vegetation modelling

We have shown that large-scale patterns in leaf N across sites can be predicted from climate based on optimality hypotheses via $V_{\text{cmax}25}$ and LMA. In complementary work, we have shown that decadal-scale, global declines in leaf and canopy N_{area} can be predicted successfully via optimality theory (Dong, Wright, et al., 2022). These findings suggest a need to revisit the mechanisms whereby N limitation is represented in coupled models of terrestrial carbon and nitrogen cycling.

Some models assume that leaf N is controlled by soil N availability, and that $V_{\text{cmax}25}$, in turn, is controlled by leaf N (see e.g. Goll et al., 2017; Walker et al., 2014; Zaehle & Dalmonech, 2011). Our findings are not consistent with this assumption. The predictable relationships of both $V_{\text{cmax}25}$ and LMA from climate indicate important controls of these traits by factors that are independent of soil N availability. Nor are these findings unique to our analysis. For example, Gvozdevaite et al. (2018), studying forests and savannas in West Africa, noted that 'there was no relationship between [soil] [N] and [K] and foliar nutrients when expressed on area basis. Foliar nutrient concentrations expressed on mass basis and plotted against soil nutrient concentration demonstrated very similar patterns ... with P being the only nutrient showing significant correlation with soil nutrients' (p. 1917).

A more promising modelling approach involves leaf-level acclimation towards optimal V_{cmax} accompanied by dynamic carbon allocation to leaves, depending on the balance of costs and benefits of N acquisition (McMurtrie & Dewar, 2013). Optimality theory also has the potential to quantify nutrient acquisition costs, thereby representing the role of soil fertility in modulating photosynthesis (Paillassa et al., 2020) and carbon allocation. Our analysis of model bias further suggests a need to extend current optimality theory to consider the effects of soil fertility on LMA.

Optimality concepts are becoming more extensively used in large-scale ecosystem and land-surface modelling, but always require empirical testing (Harrison et al., 2021). Some recent models

have implemented dynamic optimization of the partitioning of leaf N between carboxylation and electron transport (e.g. Ali et al., 2016; Haverd et al., 2018). One family of models, first introduced by Fisher et al. (2010), quantifies the relative costs of N acquisition via different pathways (including N fixation). More detailed consideration of these models, which differ substantially from one another in their assumptions, is beyond our scope. However, those empirical evaluations have been limited. In a global comparison (using a gridded dataset derived by machine learning from a large dataset of observed $V_{\text{cmax}25}$) involving both empirical and optimality-based prediction schemes, one optimality-based model (LUNA) showed a negative correlation between simulated and observed $V_{\text{cmax}25}$ (Luo et al., 2021). The model developed here is conceptually simple, parameter-sparse, and supported by independent data. Recognition of the key role of LMA in determining leaf N and successful prediction of site-mean LMA patterns are additional merits. We suggest that this approach could form the basis for a well-founded representation of C-N cycle coupling in future large-scale models.

AUTHOR CONTRIBUTIONS

Ning Dong, Iain Colin Prentice, and Ian J. Wright, conceived the study; Ning Dong, Owen K. Atkin, Keith J. Bloomfield, Tomas F. Domingues, Sean M. Gleason, Vincent Maire, Nicholas G. Smith and Han Wang contributed the gas exchange data; Ning Dong compiled the data, performed the data analyses and created all of the graphics; Ning Dong wrote initial version with significant input from Iain Colin Prentice and Ian J. Wright with all other authors contributing to subsequent versions.

ACKNOWLEDGEMENTS

This research has been supported by Australian Research Council funding to I.J.W. and I.C.P. (DP170103410), by European Research Council (ERC) funding to I.C.P. under the European Union's Horizon 2020 research and innovation programme (grant agreement No: 787203 REALM), and by the LEMONTREE (Land Ecosystem Models based On New Theory, observation and Experiments) project, funded through the generosity of Eric and Wendy Schmidt by recommendation of the Schmidt Futures programme. H.W. was supported by NSFC (32022052). T.F.D. was supported by FAPESP grant 2015/50488-5, USAID/PEER cooperative agreement number AID-OAA-A-11-00012 and the UK NERC TROBIT consortium via research grant NE/D01185x/1 to the University of Edinburgh. We thank Jon Lloyd for sharing data from TROBIT. N.G.S. acknowledges support from Texas Tech University. O.K.A. acknowledges support from Australian Research Council grants (DP130101252, CE140100008) and the Australian Government's Terrestrial Ecosystem Research Network (www.tern.org.au).

CONFLICT OF INTEREST

There is no conflict of interest.

PEER REVIEW

The peer review history for this article is available at <https://publons.com/publon/10.1111/1365-2745.13967>.

DATA AVAILABILITY STATEMENT

The compiled data are available at Zenodo <https://doi.org/10.5281/zenodo.6831903> (Dong et al., 2022a). The codes are provided at <https://doi.org/10.5281/zenodo.6301072> (Dong et al., 2022b).

ORCID

Ning Dong  <https://orcid.org/0000-0003-0793-8854>

Iain Colin Prentice  <https://orcid.org/0000-0002-1296-6764>

Ian J. Wright  <https://orcid.org/0000-0001-8338-9143>

Han Wang  <https://orcid.org/0000-0003-2482-1818>

Owen K. Atkin  <https://orcid.org/0000-0003-1041-5202>

Tomas F. Domingues  <https://orcid.org/0000-0003-2857-9838>

Sean M. Gleason  <https://orcid.org/0000-0002-5607-4741>

Vincent Maire  <https://orcid.org/0000-0002-3245-2568>

Yusuke Onoda  <https://orcid.org/0000-0001-6245-2342>

Hendrik Poorter  <https://orcid.org/0000-0001-9900-2433>

Nicholas G. Smith  <https://orcid.org/0000-0001-7048-4387>

REFERENCES

- Adams, M. A., Turnbull, T. L., Sprent, J. I., & Buchmann, N. (2016). Legumes are different: Leaf nitrogen, photosynthesis, and water use efficiency. *Proceedings of the National Academy of Sciences of the United States of America*, 113, 4098–4103.
- Ali, A. A., Xu, C., Rogers, A., Fisher, R. A., Wullschlegel, S. D., Massoud, E. C., Vrugt, J. A., Muss, J. D., McDowell, N. G., Fisher, J. B., Reich, P. B., & Wilson, C. J. (2016). A global scale mechanistic model of photosynthetic capacity (LUNA V1.0). *Geoscientific Model Development*, 9, 587–606.
- Batjes, N. H. (2016). Harmonized soil property values for broad-scale modelling (WISE30sec) with estimates of global soil carbon stocks. *Geoderma*, 269, 61–68.
- Bernacchi, C. J., Pimentel, C., & Long, S. P. (2003). In vivo temperature response functions of parameters required to model RuBP-limited photosynthesis. *Plant, Cell & Environment*, 26, 1419–1430.
- Bernacchi, C. J., Singaas, E. L., Pimentel, C., Portis, A. R., Jr., & Long, S. P. (2001). Improved temperature response functions for models of Rubisco-limited photosynthesis. *Plant, Cell & Environment*, 24, 253–259.
- Bloomfield, K. J., Domingues, T. F., Saiz, G., Bird, M. I., Crayn, D. M., Ford, A., Metcalfe, D. J., Farquhar, G. D., & Lloyd, J. (2014). Contrasting photosynthetic characteristics of forest vs. savanna species (Far North Queensland, Australia). *Biogeosciences*, 11, 7331–7347.
- Bloomfield, K. J., Prentice, I. C., Cernusak, L. A., Eamus, D., Medlyn, B. E., Rumman, R., Wright, I. J., Boer, M. M., Cale, P., Cleverly, J., Egerton, J. J. G., Ellsworth, D. S., Evans, B. J., Hayes, L. S., Hutchinson, M. F., Liddell, M. J., Macfarlane, C., Meyer, W. S., Togashi, H. F., ... Atkin, O. K. (2019). The validity of optimal leaf traits modelled on environmental conditions. *New Phytologist*, 221, 1409–1423.
- Brix, H., & Ebell, L. F. (1969). Effects of nitrogen fertilization on growth, leaf area, and photosynthesis rate in Douglas-fir. *Forest Science*, 15, 189–196.
- Burnett, A. C., Davidson, K. J., Serbin, S. P., & Rogers, A. (2019). The “one-point method” for estimating maximum carboxylation capacity of photosynthesis: A cautionary tale. *Plant, Cell & Environment*, 42, 2472–2481.
- Chen, J.-L., Reynolds, J. F., Harley, P. C., & Tenhunen, J. D. (1993). Coordination theory of leaf nitrogen distribution in a canopy. *Oecologia*, 93, 63–69.
- Davies-Barnard, T., Meyerholt, J., Zaehle, S., Friedlingstein, P., Brovkin, V., Fan, Y., Fisher, R. A., Jones, C. D., Lee, H., Peano, D., Smith, B., Wårlind,

- D., & Wiltshire, A. J. (2020). Nitrogen cycling in CIMP6 land surface models: Progress and limitations. *Biogeosciences*, 17, 5129–5148.
- Davis, T. W., Prentice, I. C., Stocker, B. D., Thomas, R. T., Whitley, R. J., Wang, H., Evans, B. J., Gallego-Sala, A. V., Sykes, M. T., & Cramer, W. (2017). Simple process-led algorithms for simulating habitats (SPLASH v.1.0): Robust indices of radiation, evapotranspiration and plant-available moisture. *Geoscientific Model Development*, 10, 689–708.
- De Kauwe, M. G., Lin, Y.-S., Wright, I. J., Medlyn, B. E., Crous, K. Y., Ellsworth, D. S., Maire, V., Prentice, I. C., Atkin, O. K., Rogers, A., Niinemets, Ü., Serbin, S. P., Meir, P., Uddling, J., Togashi, H. F., Tarvainen, L., Weerasinghe, L. K., Evans, B. J., Ishida, F. Y., & Domingues, T. F. (2016). A test of the 'one-point method' for estimating maximum carboxylation capacity from field-measured, light-saturated photosynthesis. *New Phytologist*, 210, 1130–1144.
- Dong, N., Prentice, I. C., Evans, B. J., Caddy-Retalic, S., Lowe, A. J., & Wright, I. J. (2017). Leaf nitrogen from first principles: Field evidence for adaptive variation with climate. *Biogeosciences*, 14, 481–495.
- Dong, N., Prentice, I. C., Wright, I., Wang, H., Atkin, O., Bloomfield, K., Domingues, T., Gleason, S., Maire, V., Onoda, Y., Poorter, H., & Smith, N. (2022). Data from: Leaf nitrogen from the perspective of optimal plant function (version v1). *Zenodo*, <https://doi.org/10.5281/zenodo.6831903>
- Dong, N., Prentice, I. C., Wright, I., Wang, H., Bloomfield, K., Domingues, T., Gleason, S., Maire, V., Onoda, Y., Poorter, H., & Smith, N. (2022). R scripts for 'Leaf nitrogen in the perspective of optimal plant function' (version version1). *Zenodo*, <https://doi.org/10.5281/zenodo.6301072>
- Dong, N., Prentice, I. C., Wright, I. J., Evans, B. J., Togashi, H. F., Caddy-Retalic, S., McInerney, F. A., Sparrow, B., Leitch, E., & Lowe, A. J. (2020). Components of leaf-trait variation along environmental gradients. *New Phytologist*, 228(1), 82–94.
- Dong, N., Wright, I. J., Chen, J. M., Luo, X., Wang, H., Keenan, T. F., Smith, N. G., & Prentice, I. C. (2022). Rising CO₂ and warming reduce global canopy demand for nitrogen. *New Phytologist*, in press. <https://doi.org/10.1111/nph.18076>
- Evans, J. R. (1983). Nitrogen and photosynthesis in the flag leaf of wheat (*Triticum aestivum* L.). *Plant Physiology*, 72, 297–302.
- Evans, J. R. (1989). Photosynthesis and nitrogen relationships in leaves of C3 plants. *Oecologia*, 78, 9–19.
- Evans, J. R., & Clarke, V. C. (2018). The nitrogen cost of photosynthesis. *Journal of Experimental Botany*, 70, 7–15.
- Evans, J. R., & Seemann, J. R. (1989). The allocation of protein nitrogen in the photosynthetic apparatus: Costs, consequences, and control. *Plant Biology*, 8, 183–205.
- Field, C., & Mooney, H. (1986). Photosynthesis-nitrogen relationship in wild plants. In *On the economy of plant form and function: Proceedings of the sixth Maria moors Cabot symposium, evolutionary constraints on primary productivity, adaptive patterns of energy capture in plants, Harvard Forest, Cambridge [Cambridgeshire]*. Cambridge University Press.
- Finzi, A. C., Norby, R. J., Calfapietra, C., Gallet-Budynek, A., Gielen, B., Holmes, W. E., Hoosbeek, M. R., Iversen, C. M., Jackson, R. B., Kubiske, M. E., Ledford, J., Liberloo, M., Oren, R., Polle, A., Pritchard, S., Zak, D. R., Schlesinger, W. H., & Ceulemans, R. (2007). Increases in nitrogen uptake rather than nitrogen-use efficiency support higher rates of temperate forest productivity under elevated CO₂. *Proceedings of the National Academy of Sciences of the United States of America*, 104, 14014–14019.
- Firn, J., McGree, J. M., Harvey, E., Flores-Moreno, H., Schütz, M., Buckley, Y. M., Borer, E. T., Seabloom, E. W., La Pierre, K. J., MacDougall, A. M., Prober, S. M., Stevens, C. J., Sullivan, L. L., Porter, E., Ladouceur, E., Allen, C., Moromizato, K. H., Morgan, J. W., Harpole, W. S., ... Risch, A. C. (2020). Author correction: Leaf nutrients, not specific leaf area, are consistent indicators of elevated nutrient inputs. *Nature Ecology & Evolution*, 4, 886–891.
- Fisher, J. B., Sitch, S., Malhi, Y., Fisher, R. A., Huntingford, C., & Tan, S.-Y. (2010). Carbon cost of plant nitrogen acquisition: A mechanistic, globally applicable model of plant nitrogen uptake, retranslocation, and fixation. *Global Biogeochemical Cycles*, 24, GB1014.
- Flexas, J., Niinemets, Ü., Gallé, A., Barbour, M. M., Centritto, M., Diaz-Espejo, A., Douthe, C., Galmés, J., Ribas-Carbo, M., Rodriguez, P. L., Rosselló, F., Soolanayakanahally, R., Tomas, M., Wright, I. J., Farquhar, G. D., & Medrano, H. (2013). Diffusional conductances to CO₂ as a target for increasing photosynthesis and photosynthetic water-use efficiency. *Photosynthesis Research*, 117, 45–59.
- Fontaine, C., Guimarães, P. R., Jr., Kéfi, S., Loeuille, N., Memmott, J., van der Putten, W. H., van Veen, F. J. F., & Thébault, E. (2011). The ecological and evolutionary implications of merging different types of networks. *Ecology Letters*, 14, 1170–1181.
- Franklin, O., Harrison, S. P., Dewar, R., Farrior, C. E., Brännström, Å., Dieckmann, U., Pietsch, S., Falster, D., Cramer, W., Loreau, M., Wang, H., Mäkelä, A., Rebel, K. T., Meron, E., Schymanski, S. J., Rovenskaya, E., Stocker, B. D., Zaehle, S., Manzoni, S., ... Prentice, I. C. (2020). Organizing principles for vegetation dynamics. *Nature Plants*, 6, 444–453.
- Givnish, T. (1979). On the adaptive significance of leaf form. In O. T. Solbrig, S. Jain, G. B. Johnson, & P. H. Raven (Eds.), *Topics in plant population biology* (pp. 375–407). Macmillan.
- Givnish, T. (1987). Comparative studies of leaf form: Assessing the relative roles of selective pressures and phylogenetic constraints. *New Phytologist*, 106, 131–160.
- Goll, D. S., Vuichard, N., Maignan, F., Jornet-Puig, A., Sardans, J., Violette, A., Peng, S., Sun, Y., Kvakic, M., Guimberteau, M., Guenet, B., Zaehle, S., Penuelas, J., Janssens, I., & Ciais, P. (2017). A representation of the phosphorus cycle for ORCHIDEE (revision 4520). *Geoscientific Model Development*, 10, 3745–3770.
- Gvozdevaite, A., Oliveras, I., Domingues, T. F., Peprah, T., Boakye, M., Afriyie, L., da Silva Peixoto, K., de Farias, J., Almeida de Oliveira, E., Almeida Farias, C. C., dos Santos Prestes, N. C. C., Neyret, M., Moore, S., Schwantes Marimon, B., Marimon Junior, B. H., Adu-Bredu, S., & Malhi, Y. (2018). Leaf-level photosynthetic capacity dynamics in relation to soil and foliar nutrients along forest-savanna boundaries in Ghana and Brazil. *Tree Physiology*, 38, 1926.
- Harrison, S., Cramer, W., Franklin, O., Prentice, I. C., Wang, H., Brannstrom, A., de Boer, H., Dieckmann, U., Joshi, J., Keenan, T., Lavergne, A., Manzoni, S., Mengoli, G., Morfopoulos, C., Penuelas, J., Dietsch, S., Rebel, K., Ryu, Y., Smith, N., ... Wright, I. (2021). Eco-evolutionary optimality as a means to improve vegetation and land-surface models. *New Phytologist*, 231, 2125–2141.
- Haverd, V., Smith, B., Nieradzki, L., Briggs, P. R., Woodgate, W., Trudinger, C. M., Canadell, J. G., & Cuntz, M. (2018). A new version of the CABLE land surface model (subversion revision r4601) incorporating land use and land cover change, woody vegetation demography, and a novel optimisation-based approach to plant coordination of photosynthesis. *Geoscientific Model Development*, 11, 2995–3026.
- Jiang, C., Ryu, Y., Wang, H., & Keenan, T. F. (2020). An optimality-based model explains seasonal variation in C3 plant photosynthetic capacity. *Global Change Biology*, 26, 6493–6510.
- Karger, D. N., Conrad, O., Böhner, J., Kawohl, T., Kreft, H., Soria-Auza, R. W., Zimmermann, N. E., Linder, H. P., & Kessler, M. (2017). Climatologies at high resolution for the earth's land surface areas. *Scientific Data*, 4, 170122.
- Kattge, J., Bönsch, G., Díaz, S., Lavorel, S., Prentice, I. C., Leadley, P., Tautenhahn, S., Werner, G. D. A., Aakala, T., Abedi, M., Acosta, A. T. R., Adamidis, G. C., Adamson, K., Aiba, M., Albert, C. H., Alcántara, J. M., Alcázar, C., Aleixo, I., Ali, H., ... Wirth, C. (2020). TRY plant trait database – Enhanced coverage and open access. *Global Change Biology*, 26, 119–188.

- Keenan, T. F., & Niinemets, Ü. (2016). Global leaf trait estimates biased due to plasticity in the shade. *Nature Plants*, 3, 16201.
- Kikuzawa, K. (1991). A cost-benefit analysis of leaf habit and leaf longevity of trees and their geographical pattern. *The American Naturalist*, 138, 1250–1263.
- Kikuzawa, K., Seiwa, K., & Lechowicz, M. J. (2013). Leaf longevity as a normalization constant in allometric predictions of plant production. *PLoS ONE*, 8, e81873.
- Li, W., Zhang, H., Huang, G., Liu, R., Wu, H., Zhao, C., & McDowell, N. G. (2020). Effects of nitrogen enrichment on tree carbon allocation: A global synthesis. *Global Ecology and Biogeography*, 29, 573–589.
- Liang, X., Zhang, T., Lu, X., Ellsworth, D. S., BassiriRad, H., You, C., Wang, D., He, P., Deng, Q., Liu, H., Mo, J., & Ye, Q. (2020). Global response patterns of plant photosynthesis to nitrogen addition: A meta-analysis. *Global Change Biology*, 26, 3585–3600.
- Luo, X., Keenan, T. F., Chen, J. M., Croft, H., Prentice, I. C., Smith, N. G., Walker, A. P., Wang, H., Wang, R., Xu, C., & Zhang, Y. (2021). Global variation in the fraction of leaf nitrogen allocated to photosynthesis. *Nature Communications*, 12, 4866.
- Luo, Y., Su, B., Currie, W. S., Dukes, J. S., Finzi, A., Hartwig, U., Hungate, B., McMurtrie, R. E., Oren, R., Parton, W. J., Pataki, D. E., Shaw, R. M., Zak, D. R., & Field, C. B. (2004). Progressive nitrogen limitation of ecosystem responses to rising atmospheric carbon dioxide. *Bioscience*, 54, 731–739.
- Maire, V., Soussana, J.-F., Gross, N., Bachelet, B., Pagès, L., Martin, R., Reinhold, T., Wirth, C., & Hill, D. (2013). Plasticity of plant form and function sustains productivity and dominance along environment and competition gradients. A modeling experiment with Gemini. *Ecological Modelling*, 254, 80–91.
- Maire, V., Wright, I. J., Prentice, I. C., Batjes, N. H., Bhaskar, R., van Bodegom, P. M., Cornwell, W. K., Ellsworth, D., Niinemets, Ü., & Ordonez, A. (2015). Global effects of soil and climate on leaf photosynthetic traits and rates. *Global Ecology and Biogeography*, 24, 706–717.
- McMurtrie, R. E., & Dewar, R. C. (2013). New insights into carbon allocation by trees from the hypothesis that annual wood production is maximized. *New Phytologist*, 199, 981–990.
- Medlyn, B. E., Zaehle, S., De Kauwe, M. G., Walker, A. P., Dietze, M. C., Hanson, P. J., Hickler, T., Jain, A. K., Luo, Y., Parton, W., Prentice, I. C., Thornton, P. E., Wang, S., Wang, Y.-P., Weng, E., Iversen, C. M., McCarthy, H. R., Warren, J. M., Oren, R., & Norby, R. J. (2015). Using ecosystem experiments to improve vegetation models. *Nature Climate Change*, 5, 528–534.
- Meyerholt, J., Sickel, K., & Zaehle, S. (2020). Ensemble projections elucidate effects of uncertainty in terrestrial nitrogen limitation on future carbon uptake. *Global Change Biology*, 26, 3978–3996.
- Niinemets, Ü. (1999). Research review. Components of leaf dry mass per area – Thickness and density – Alter leaf photosynthetic capacity in reverse directions in woody plants. *New Phytologist*, 144, 35–47.
- Norby, R. J., Warren, J. M., Iversen, C. M., Medlyn, B. E., & McMurtrie, R. E. (2010). CO₂ enhancement of forest productivity constrained by limited nitrogen availability. *Proceedings of the National Academy of Sciences of the United States of America*, 107, 19368–19373.
- Onoda, Y., Wright, I. J., Evans, J. R., Hikosaka, K., Kitajima, K., Niinemets, Ü., Poorter, H., Tosens, T., & Westoby, M. (2017). Physiological and structural tradeoffs underlying the leaf economics spectrum. *New Phytologist*, 214, 1447–1463.
- Osnas, J. L. D., Katabuchi, M., Kitajima, K., Wright, S. J., Reich, P. B., Bael, S. A. V., Kraft, N. J. B., Samaniego, M. J., Pacala, S. W., & Lichstein, J. W. (2018). Divergent drivers of leaf trait variation within species, among species, and among functional groups. *Proceedings of the National Academy of Sciences of the United States of America*, 115, 5480–5485.
- Osnas, J. L. D., Lichstein, J. W., Reich, P. B., & Pacala, S. W. (2013). Global leaf trait relationships: Mass, area, and the leaf economics spectrum. *Science*, 340, 741–744.
- Osone, Y., Ishida, A., & Tateno, M. (2008). Correlation between relative growth rate and specific leaf area requires associations of specific leaf area with nitrogen absorption rate of roots. *New Phytologist*, 179, 417–427.
- Paillassa, J., Wright, I. J., Prentice, I. C., Pepin, S., Smith, N. G., Ethier, G., Westerband, A. C., Lamarque, L. J., Wang, H., Cornwell, W. K., & Maire, V. (2020). When and where soil is important to modify the carbon and water economy of leaves. *New Phytologist*, 228, 121–135.
- Peng, Y., Bloomfield, K. J., Cernusak, L. A., Domingues, T., & Prentice, I. C. (2021). Global climate and nutrient controls of photosynthetic capacity. *Communications Biology*, 4, 462.
- Peng, Y., Bloomfield, K. J., & Prentice, I. C. (2020). A theory of plant function helps to explain leaf-trait and productivity responses to elevation. *New Phytologist*, 226, 1274–1284.
- Poorter, H., Niinemets, Ü., Ntagkas, N., Siebenkäs, A., Mäenpää, M., Matsubara, S., & Pons, T. (2019). A meta-analysis of plant responses to light intensity for 70 traits ranging from molecules to whole plant performance. *New Phytologist*, 223, 1073–1105.
- Prentice, I. C., Dong, N., Gleason, S. M., Maire, V., Wright, I. J., & Penuelas, J. (2014). Balancing the costs of carbon gain and water transport: Testing a new theoretical framework for plant functional ecology. *Ecology Letters*, 17, 82–91.
- R Core Team. (2020). *R: A language and environment for statistical computing*. R Foundation for Statistical Computing. Retrieved from <https://www.R-project.org/>
- Scafaro, A. P., Xiang, S., Long, B. M., Bahar, N. H. A., Weerasinghe, L. K., Creek, D., Evans, J. R., Reich, P. B., & Atkin, O. K. (2017). Strong thermal acclimation of photosynthesis in tropical and temperate wet-forest tree species: The importance of altered Rubisco content. *Global Change Biology*, 23, 2783–2800.
- Skillman, J. B. (2008). Quantum yield variation across the three pathways of photosynthesis: Not yet out of the dark. *Journal of Experimental Botany*, 59, 1647–1661.
- Smith, N. G., & Keenan, T. F. (2020). Mechanisms underlying leaf photosynthetic acclimation to warming and elevated CO₂ as inferred from least-cost optimality theory. *Global Change Biology*, 26, 5202–5216.
- Smith, N. G., Keenan, T. F., Prentice, I. C., Wang, H., Wright, I. J., Niinemets, Ü., Crous, K. Y., Domingues, T. F., Guerrieri, R., Yoko Ishida, F., Kattge, J., Kruger, E. L., Maire, V., Rogers, A., Serbin, S. P., Tarvainen, L., Togashi, H. F., Townsend, P. A., Wang, M., ... Zhou, S.-X. (2019). Global photosynthetic capacity is optimized to the environment. *Ecology Letters*, 22, 506–517.
- Stitt, M., & Schulze, D. (1994). Does rubisco control the rate of photosynthesis and plant growth? An exercise in molecular ecophysiology. *Plant, Cell & Environment*, 17, 465–487.
- Stocker, B. D., Wang, H., Smith, N. G., Harrison, S. P., Keenan, T. F., Sandoval, D., Davis, T., & Prentice, I. C. (2020). P-model v1.0: An optimality-based light use efficiency model for simulating ecosystem gross primary production. *Geoscientific Model Development*, 13, 1545–1581.
- Togashi, H., Prentice, I. C., Atkin, O. K., Macfarlane, C., Prober, S. M., Bloomfield, K. J., & Evans, B. J. (2018). Thermal acclimation of leaf photosynthetic traits in an evergreen woodland, consistent with the coordination hypothesis. *Biogeosciences*, 15, 3461–3474.
- Walker, A. P., Beckerman, A. P., Gu, L., Kattge, J., Cernusak, L. A., Domingues, T. F., Scales, J. C., Wohlfahrt, G., Wullschlegel, S. D., & Woodward, F. I. (2014). The relationship of leaf photosynthetic traits – V_{cmax} and J_{max} – To leaf nitrogen, leaf phosphorus, and specific leaf area: A meta-analysis and modeling study. *Ecology and Evolution*, 4, 3218–3235.
- Wang, H., Atkin, O. K., Keenan, T. F., Smith, N. G., Wright, I. J., Bloomfield, K. J., Kattge, J., Reich, P. B., & Prentice, I. C. (2020). Acclimation of

- leaf respiration consistent with optimal photosynthetic capacity. *Global Change Biology*, 26, 2573–2583.
- Wang, H., Prentice, I. C., Keenan, T. F., Davis, T. W., Wright, I. J., Cornwell, W. K., Evans, B. J., & Peng, C. (2017). Towards a universal model for carbon dioxide uptake by plants. *Nature Plants*, 3, 734–741.
- Wang, H., Prentice, I. C., Wright, I. J., Qiao, S., Xu, X., Kikuzawa, K., & Stenseth, N. C. (2021). Leaf economics explained by optimality principles. *bioRxiv*, 2021.02.07.430028.
- Warren, C. R., & Adams, M. A. (2001). Distribution of N, Rubisco and photosynthesis in *Pinus pinaster* and acclimation to light. *Plant, Cell & Environment*, 24, 597–609.
- Weedon, G. P., Balsamo, G., Bellouin, N., Gomes, S., Best, M. J., & Viterbo, P. (2014). The WFDEI meteorological forcing data set: WATCH forcing data methodology applied to ERA-interim reanalysis data. *Water Resources Research*, 50, 7505–7514.
- Wright, I. J., Reich, P. B., Cornelissen, J. H. C., Falster, D. S., Garnier, E., Hikosaka, K., Lamont, B. B., Lee, W., Oleksyn, J., Osada, N., Poorter, H., Villar, R., Warton, D. I., & Westoby, M. (2005). Assessing the generality of global leaf trait relationships. *New Phytologist*, 166, 485–496.
- Wright, I. J., Reich, P. B., Westoby, M., Ackerly, D. D., Baruch, Z., Bongers, F., Cavender-Bares, J., Chapin, T., Cornelissen, J. H. C., Diemer, M., Flexas, J., Garnier, E., Groom, P. K., Gulias, J., Hikosaka, K., Lamont, B. B., Lee, T., Lee, W., Lusk, C., ... Villar, R. (2004). The worldwide leaf economics spectrum. *Nature*, 428, 821–827.
- Xu, H., Wang, H., Prentice, I. C., Harrison, S. P., Wang, G., & Sun, X. (2021). Predictability of leaf traits with climate and elevation: A case study in Gongga Mountain, China. *Tree Physiology*, 41(8), 1336–1352. <https://doi.org/10.1093/treephys/tpab003>
- Yang, G., Peng, Y., Abbott, B. W., Biasi, C., Wei, B., Zhang, D., Wang, J., Yu, J., Li, F., Wang, G., Kou, D., Liu, F., & Yang, Y. (2021). Phosphorus rather than nitrogen regulates ecosystem carbon dynamics after permafrost thaw. *Global Change Biology*, 27, 5818–5830. <https://doi.org/10.1111/gcb.15845>
- Zaehle, S., & Dalmonech, D. (2011). Carbon–nitrogen interactions on land at global scales: Current understanding in modelling climate biosphere feedbacks. *Current Opinion in Environmental Sustainability*, 3, 311–320.
- Zaehle, S., Medlyn, B. E., De Kauwe, M. G., Walker, A. P., Dietze, M. C., Hickler, T., Luo, Y., Wang, Y.-P., El-Masri, B., Thornton, P., Jain, A., Wang, S., Warland, D., Weng, E., Parton, W., Iversen, C. M., Gallet-Budynek, A., McCarthy, H., Finzi, A., ... Norby, R. J. (2014). Evaluation of 11 terrestrial carbon–nitrogen cycle models against observations from two temperate free-air CO₂ enrichment studies. *New Phytologist*, 202, 803–822.
- Zhu, Z., Bi, J., Pan, Y., Ganguly, S., Anav, A., Xu, L., Samanta, A., Piao, S., Nemani, R. R., & Myneni, R. B. (2013). Global data sets of vegetation leaf area index (LAI) 3g and fraction of photosynthetically active radiation (FPAR) 3g derived from global inventory modeling and mapping studies (GIMMS) normalized difference vegetation index (NDVI3g) for the period 1981 to 2011. *Remote Sensing*, 5, 927–948.

SUPPORTING INFORMATION

Additional supporting information can be found online in the Supporting Information section at the end of this article.

How to cite this article: Dong, N., Prentice, I. C., Wright, I. J., Wang, H., Atkin, O. K., Bloomfield, K. J., Domingues, T. F., Gleason, S. M., Maire, V., Onoda, Y., Poorter, H., & Smith, N. G. (2022). Leaf nitrogen from the perspective of optimal plant function. *Journal of Ecology*, 110, 2585–2602. <https://doi.org/10.1111/1365-2745.13967>